

54

62 64276

Copy 412
RM L57C11

NACA RM L57C11

Code-1



CLASSIFICATION CHANGED TO
DECLASSIFIED EFFECTIVE
12 MARCH 63 AUTHORITY
NACA CON 3 BY J.J. CARROLL

N63-14763

RESEARCH MEMORANDUM

EFFECT OF HINGE-LINE POSITION ON THE OSCILLATING
HINGE MOMENTS AND FLUTTER CHARACTERISTICS OF
A FLAP-TYPE CONTROL AT TRANSONIC SPEEDS

By Robert F. Thompson and William C. Moseley, Jr.

Langley Aeronautical Laboratory
Langley Field, Va.

OTS PRICE

XEROX	\$	<u>5.60 pb</u>
MICROFILM	\$	<u>1.82 my</u>

CLASSIFIED DOCUMENT

This material contains information affecting the National Defense of the United States within the meaning of the espionage laws, Title 18, U.S.C., Secs. 793 and 794, the transmission or revelation of which in any manner to an unauthorized person is prohibited by law.

NATIONAL ADVISORY COMMITTEE FOR AERONAUTICS

WASHINGTON

June 10, 1957

~~CONFIDENTIAL~~



NATIONAL ADVISORY COMMITTEE FOR AERONAUTICS

RESEARCH MEMORANDUM

EFFECT OF HINGE-LINE POSITION ON THE OSCILLATING
HINGE MOMENTS AND FLUTTER CHARACTERISTICS OF
A FLAP-TYPE CONTROL AT TRANSONIC SPEEDS

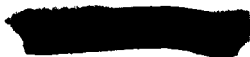
By Robert F. Thompson and William C. Moseley, Jr.

SUMMARY

14763

Free-oscillation tests were made to determine the dynamic hinge-moment characteristics of a trailing-edge, flap-type control surface with various hinge-line positions. The essentially full-span control was tested on a 4-percent-thick, low-aspect-ratio wing as a reflection plane configuration in the Langley high-speed 7- by 10-foot tunnel. The total control chord was 30 percent of the wing chord, and ratios of balance chord to flap chord rearward of the hinge line of 0.20, 0.35, and 1.00 are reported. Test parameters covered a Mach number range from 0.40 to 1.02, control oscillating amplitudes of about 10° or larger, angles of attack of 0° and 6° , and a range of control reduced frequencies. Static data were also obtained for the three control hinge-line positions and results are compared with existing theories.

Results show that oscillating amplitude has a large effect on the control aerodynamic damping derivative and that the damping is unstable in the test Mach number range above about 0.90 for the hinge positions tested. Damping was generally stable at Mach numbers below 0.90 although it was unstable at subsonic speeds for high oscillation amplitudes of the control hinged at the midchord. When the total damping of the control system (nonaerodynamic plus aerodynamic) was unstable, the control fluttered with only one degree of freedom and at transonic speeds the flutter amplitude was decreased by a rearward movement of the hinge line. Test variations in angle of attack and control reduced frequency had little effect on the oscillating hinge-moment derivatives $C_{h\delta, \omega}$ and $C_{h\dot{\delta}, \omega}$. Considering existing limitations, good agreement was obtained with results computed by two-dimensional, potential-flow theory.



INTRODUCTION

Aerodynamic hinge-moment data for flap-type controls determined under oscillatory conditions are needed in flutter and servocontrol analyses. At present, theoretical calculations of these moments are generally considered unsatisfactory at transonic speeds and little experimental data are available for these conditions. However, a few results exist which cover certain features of the transonic behavior of these controls.

One of the more important factors affecting the hinge-moment characteristic of the control is the location of the hinge axis. Experimental results reported in reference 1 show that the rotational aerodynamic damping of a flap-type control is unstable at transonic speeds for a control with the hinge line located a moderate distance from the leading edge of the control. However, theoretical work reported in reference 2 shows the rotational damping of a wing alone to be stable at low supersonic speeds for a rotational axis rearward of the 0.66-chord point of the control. Therefore, it was felt possible that flap-type controls with substantial amounts of aerodynamic balance would have favorable aerodynamic damping characteristics in the transonic region.

The purpose of the present investigation was to determine the effects of hinge-line position on the dynamic hinge-moment and flutter characteristics of a flap-type control surface at transonic speeds. In view of the results of reference 2, it was considered of interest to obtain these data with the hinge line located fairly far rearward, even though this factor reduces the control effectiveness and makes it statically unstable. (See ref. 3.)

This investigation was basically an extension of the work reported in reference 1. The wing-control model was essentially the same and was originally intended to be a 1/8-scale model of the X-1E research airplane wherein the model included only the outboard 35 percent of the wing semi-span. For the present tests, the control hinge line was shifted rearward relative to the hinge-line location of the control reported in reference 1.

Oscillating hinge moments and associated flutter characteristics were determined for a range of control reduced frequencies and two setback hinge positions. Static hinge moments were also obtained. The effects of angle of attack and control-surface oscillating amplitude were investigated over a Mach number range from about 0.40 to 1.02. In addition, pertinent results from reference 1, which are considered directly comparable, were used to extend the range of hinge-line positions reported herein.

SYMBOLS

C_h	control hinge-moment coefficient, $\frac{\text{Hinge moment}}{2M'q}$
M'	area moment of control area rearward of and about hinge line, ft^3
q	free-stream dynamic pressure, lb/sq ft
M_h	aerodynamic hinge moment on control per unit deflection, positive trailing edge down, ft-lb/radian
c	local wing chord, ft
c_a	control chord (distance from hinge line rearward to trailing edge of control, see fig. 1), ft
c_b	balance chord (distance from hinge line forward to leading edge of control, see fig. 1), ft
c_t	total control chord, $c_a + c_b$, ft
k	reduced frequency, $\omega c_t / 2V$, with c_t taken at midspan of control
ω	angular frequency of oscillation, $2\pi f$, radians/sec
f	frequency of oscillation, cps
f_0	control wind-off natural frequency, cps
V	free-stream velocity, ft/sec
I	moment of inertia of control system, slug-ft^2
λ	logarithmic decrement, $\frac{d(\log \delta_1)}{d(\text{time})}$, per second
δ_1	amplitude of oscillation, deg to each side of mean
δ	control-surface deflection, measured in a plane perpendicular to control-surface hinge line, positive when control-surface trailing edge is below wing chord plane, radians except as noted



- M effective Mach number over span of model, $\frac{2}{S_1} \int_0^{b/2} cM_a dy$
- S_1 twice wing area of semispan model, sq ft
- b twice span of semispan model, ft
- M_a average chordwise local Mach number
- M_l local Mach number
- y spanwise distance from plane of symmetry, ft
- α angle of attack of wing chord plane, deg

$$C_{h\delta} = \frac{\partial C_h}{\partial \delta}$$

$$C_{h\delta,\omega} = \frac{\text{Real part of } M_{\delta}}{2M'q}, \text{ per radian}$$

$$C_{h\delta,\omega}^i = \frac{\text{Imaginary part of } M_{\delta}}{2M'qk}, \text{ per radian}$$

the subscript ω indicates derivatives that are a function of ω

- θ phase angle of resultant aerodynamic moment with respect to the control displacement, $\tan \theta = \frac{kC_{h\delta,\omega}^i}{C_{h\delta,\omega}}, \text{ deg}$
- B "bumped" flutter condition, flutter starts when the control surface is manually displaced and suddenly released
- S "self-starting" flutter condition, flutter starts due to random tunnel disturbances when the control is released at 0° deflection

MODEL AND APPARATUS

The test model consisted of a semispan wing, a flap-type control surface, and a torsion spring and deflector mechanism as shown in the schematic drawing in figure 1. General model dimensions are given in figure 2, and photographs are shown in figure 3. The model was designed





so that the internal damping and spring constant of the control system could be varied and was tested as a reflection plane configuration at transonic Mach numbers in the Langley high-speed 7- by 10-foot tunnel.

Wing Details

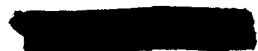
The wing had an aspect ratio of 1.80, a taper ratio of 0.74, and an NACA 64A004 airfoil section with a modified trailing edge. The portion of the wing rearward of the 70-percent-chord line was modified so that the trailing edge had a constant thickness equal to 0.0036c. This trailing-edge modification was based on construction consideration for the X-1E airplane and carried over to this investigation to keep results comparable with reference 1.

The wing was constructed with a steel core and a plastic surface. All oscillation tests were made with a tip store added to the wing. Details of the tip store are shown in figure 1 and table I. Two geometrically similar stores having vastly different weights were used to vary the wing natural frequencies for various test conditions. The natural first bending and torsion frequencies of the wing, with the light and the heavy tip store, are given in table II. These frequencies were obtained with the torsion spring clamped at 8.2 inches from the reference position (fig. 4) and are average values for the two controls since shifting the hinge line had a slight effect on the wing frequencies.

Control-System Details

The total chord of the control was 30 percent of the local wing chord and the span of the control extended from the 0.086b/2 model station to the 0.943b/2 model station. Two setback hinge-line positions were tested and the ratios of balance chord to control chord rearward of the hinge line were 0.35 and 1.00 (fig. 2). The gap between the control nose and wing was unsealed. The controls were statically mass balanced with the balance distributed so as to balance as near as possible each spanwise segment. They were made of steel and the $c_b/c_a = 0.35$ control was balanced by a tungsten nose insert and holes drilled perpendicular to the chord plane rearward of the hinge line (fig. 3(b)). The $c_b/c_a = 1.00$ control was balanced by holes drilled forward of the hinge line (fig. 3(c)). These holes were plugged with balsa and the entire control surface covered with silk.

The inboard tang of the control extended through the reflection plane to the outside of the tunnel (fig. 1). The tang extension consisted of a damper rod and a torsion spring. The control was mounted by two ball bearings outside the tunnel and a plain bearing at the wing



tip. The system was carefully aligned to keep friction to a minimum. Attached to the damper rod was a small armature which rotated in the magnetic field of a reluctance-type pickup to indicate control position and a deflection arm used to apply a step deflection to the control system. A movable clamp was used to vary the length of the torsion spring and hence the natural frequency of the control system. The values of natural frequency are given in figure 4 for each clamp position. The moments of inertia of the control system with the two controls are given in table III. The viscous damper used to increase the tare damping of the system is described in reference 1 and was used in this investigation for only a few test points.

INSTRUMENTATION

Strain gages were located near the root of the wing to indicate the wing bending and torsion response. Control deflection was measured by a reluctance-type pickup located at the end of the damper rod nearest the control. These three quantities were recorded against time by a recording oscillograph. Dynamic calibration of the recording system indicated accurate response to a frequency of about 500 cycles per second.

TESTS

The tests were made in the Langley high-speed 7- by 10-foot tunnel utilizing the side-wall reflection-plane test technique. This technique involves the mounting of a relatively small model on a reflection plate spaced out from the tunnel wall to bypass the tunnel boundary layer. Local velocities over the surface of the test reflection plate allow testing to a Mach number of about 1.02 without choking the tunnel.

Typical contours of local Mach number, in the vicinity of the model location obtained with no model in place, are shown in figure 5. Average test Mach numbers were obtained from similar contour charts by using the relationship

$$M = \frac{2}{S_1} \int_0^{b/2} cM_a dy$$

The tunnel stagnation pressure was essentially equal to sea-level atmospheric conditions.



The variation of Reynolds number based on the wing mean aerodynamic chord with test Mach number is presented in figure 6. The width of the band in figure 6 represents, for these tests at a given Mach number, the maximum variation of Reynolds number with atmospheric conditions.

Oscillating hinge moments were obtained for amplitudes up to about 10° or larger through a Mach number range of about 0.40 to 1.02. These data were measured at $\alpha = 0^\circ$ for both hinge-line positions tested and at $\alpha = 6^\circ$ for the $c_b/c_a = 1.00$ control. The control reduced-frequency range varied with control hinge-line position and Mach number and was generally in the range from 0.05 to 0.25. In addition, static hinge-moment data were obtained at $\alpha = 0^\circ$ for both controls and at $\alpha = 6^\circ$ for the $c_b/c_a = 0.35$ control.

TEST TECHNIQUE AND REDUCTION OF DATA

Oscillating hinge moments were obtained from the free-oscillation response of the control system. The control system was designed so that at the test frequencies the torsional response of the control about the hinge line was essentially that of a single-degree-of-freedom system. The wing response characteristics were varied relative to the control oscillating frequency so that the physical response of the model for the various test conditions was predominantly control rotation. Therefore, the aerodynamic moment resulting from angular deflection of the control about the hinge line could be determined from the free-oscillation characteristics of the control system following known starting conditions. Typical oscillograph records of the time response of the model are shown in figure 7.

The technique used to initiate the free oscillations depended on the total damping (aerodynamic plus nonaerodynamic) of the control system for the particular test condition. The term "nonaerodynamic" is considered to include the system frictional and structural damping plus any artificial damping that might be added. When the total damping was unstable at low deflections, the hinge moments were determined from the unstable oscillation following release of the control at $\delta = 0^\circ$ (fig. 7(c)). This type of oscillation was initiated by random tunnel disturbances and in all cases was self-limiting because of the nonlinear variation of aerodynamic damping with oscillating amplitude. When the total damping was stable or varied from stable to unstable within the test oscillation amplitude range, the free oscillation was initiated by releasing the control at some initial deflection angle at zero initial rotational velocity (figs. 7(a) and 7(b)). The ensuing oscillation was either a buildup or a decay and for the conditions where the damping varied from stable to unstable, the initial deflection angle was changed

so as to study the complete oscillation amplitude range. In addition, a very small portion of the data was determined from decayed oscillations made stable by increasing the nonaerodynamic damping of the system with the viscous damper.

The hinge moment existing on an oscillating control is not necessarily in phase with the control position and may be represented in complex notation by the relation

$$\frac{M_{\delta}}{2M'q} = C_{h_{\delta},\omega} + ikC_{h_{\delta},\omega} \quad (1)$$

The part $C_{h_{\delta},\omega}$ is proportional to the real component of the moment which is commonly called the in-phase or spring moment. The part $kC_{h_{\delta},\omega}$ is proportional to the imaginary component of the moment which is commonly called the out-of-phase or damping moment. Frequency effects higher than first order could not be separated by the test method used in this investigation; therefore, the parameters $C_{h_{\delta},\omega}$ and $kC_{h_{\delta},\omega}$ include the higher order derivatives that are either in-phase or out-of-phase, respectively, with control position.

Evaluation of Spring Moments

The aerodynamic in-phase or spring moment was determined from the natural frequency of oscillation of the control system. Since the variation of in-phase moment is not necessarily linear with amplitude and the test method was not sufficiently accurate to determine the variation in natural frequency with amplitude, the values of $C_{h_{\delta},\omega}$ presented are effective values averaged over the amplitude range of the oscillation. The effect of the values of damping encountered in this investigation on the natural frequency was considered negligible and the aerodynamic spring-moment derivative was determined from the relationship

$$C_{h_{\delta},\omega} = \frac{I(\omega_o^2 - \omega^2)}{2M'q} \quad (2)$$

where the subscript o signifies a wind-off condition. As shown by equation (2), negative values of $C_{h_{\delta},\omega}$ oppose the control displacement and hence increase the stiffness or natural frequency of the control system.

Evaluation of Damping Moments

The aerodynamic out-of-phase or damping moment was determined from the rate of buildup or decay of the free oscillation of the control system. Like the spring moment, the damping moment is not necessarily linear with amplitude and the damping results were analyzed on the basis of an equivalent linear system. It was assumed that all damping forces considered in this investigation were adequately described by an equivalent viscous damping and the time response of the actual system was simulated by a linear system having the appropriate damping constant at each oscillating amplitude for a given frequency. The variation of damping-moment parameter with oscillating amplitude was obtained by plotting the logarithm of the amplitude of successive cycles of the oscillation against time and taking, at a particular amplitude, the slope of the faired curve through the points as the value of the logarithmic decrement $\lambda = \frac{d(\log \delta_1)}{d(\text{time})}$ of the oscillation at that amplitude.

The aerodynamic damping-moment derivative was determined from the relationship

$$C_{h\delta, \omega} = \frac{2IV}{qM'c_t} (\lambda - \lambda_0) \quad (3)$$

where the subscript 0 refers to wind-off values taken at approximately the same frequency and amplitude as the wind-on values.

The aerodynamic damping derivative is related to an equivalent viscous damping constant $(C, \frac{\text{ft-lb}}{\text{rad/sec}})$ by the expression

$$C = C_{h\delta, \omega} \frac{c_t q M'}{V} \quad (4)$$

Determination of Static Hinge Moments

Static hinge moments were measured by attaching a clamp to the control system at the damper rod. This clamp replaced the oscillating spring clamp and was fitted with a calibrated electric strain gage which measured the torque about the control hinge line for various control deflections. The static hinge-moment coefficient C_h was determined from the relationship

$$C_h = \frac{\text{Torque}}{2M'q} \quad (5)$$



General Comments

Values given for oscillating and flutter amplitudes are to each side of mean and for this investigation the mean oscillating amplitude was very near zero deflection. Therefore, the oscillating and flutter amplitudes correspond closely to the control amplitude measured relative to the wing-chord plane. Flutter in all cases was a limited amplitude oscillatory condition and was terminated by physically restraining the control motion. For the free-oscillation technique used, the oscillation reduced frequency k varies with Mach number and values of k are given for each Mach number.

The wing bending and torsion traces shown in figure 7 are a measure of the wing root bending and torsion stresses, whereas the control position trace indicates the control deflection. The traces in figures 7(a) and 7(b) were more sensitive than those in 7(c). It would be desirable to eliminate all wing motion in an investigation of this type but this is not practical. However, care was taken to minimize the wing motion. The control surface was dynamically balanced about the hinge line to prevent any inertia coupling between the wing and control due to control rotation, and the wing was fitted with a tip store of variable mass to control the wing response motion to the control-induced aerodynamic forcing function. Wing bending and torsion responses of the general magnitude encountered in these tests were approximated by simple wing translation and rotation and analyzed by the theoretical methods presented in references 4 and 5. The effects of this wing motion on the calculated control hinge-moment parameters for a control hinged at the leading edge was very small. Therefore, in this investigation, wing motion was considered to have only secondary effects on the control hinge-moment parameters.

The control-system response was nonlinear due to the fact that the aerodynamic spring and damping-moment derivatives depended on the control displacement. Some compromise of the actual aerodynamic spring and damping constants of the system was undoubtedly made by the methods used to analyze the nonlinear system. This compromise is expected to be larger for the spring moments than for the damping moments. However, it is believed that for the range of physical constants of these tests, the method of analysis gives sufficient accuracy for practical purposes.

CORRECTIONS

No corrections have been applied to the data for the chordwise and spanwise velocity gradients or for the effects of the tunnel walls. It is shown in reference 6 that a tunnel resonance phenomenon can appreciably decrease the magnitude of forces and moments measured in

oscillation tests. However, it is believed that this phenomenon had no appreciable effect on the results of the present investigation. In general, most of the test frequencies were well removed from the calculated resonant frequencies and there was no apparent decrease in moments for the test frequencies that were close to resonant frequencies. It is possible that the magnitude of the resonant effects would be relieved by the model tip effects and the nonuniformity of the velocity field in the test section.

Static control-deflection corrections have been applied to the output of the position pickup to give the deflection at the midspan of the control surface. No dynamic corrections were applied to account for the twist of the control system outboard of the position pickup (fig. 4) since, for the physical constants and frequencies involved, this was a secondary effect and generally negligible.

RESULTS AND DISCUSSION

Presentation of Data

Static hinge-moment data are presented in figures 8 and 9. The variation of aerodynamic damping derivative $C_{h\delta,\omega}$ with oscillating amplitude and Mach number together with the associated flutter characteristics are presented in figures 10 to 12 for the complete range of this investigation. The variation of the aerodynamic spring derivative $C_{h\delta,\omega}$ with Mach number for the various test wind-off frequencies is shown in figures 13 and 14 and a comparison between static and dynamic spring-moment results is presented in figure 15. Figure 16 shows the effect of hinge-line position on the oscillating hinge-moment derivatives for various Mach numbers, and figure 17 compares the effect of hinge-line position on the static and dynamic hinge-moment parameters as determined by experiment and theory. Figures 18 and 19 give additional comparison of the experimental oscillating hinge-moment results with theory. Figure 20 shows the effect of hinge-line position, Mach number, and reduced frequency on the resultant aerodynamic hinge-moment vector.

The $c_b/c_a = 0.20$ control reported in reference 1 and used herein in figures 16 to 20 for comparison was tested on the wing without a tip store and the overhang nose span was slightly different from the present controls; however, these effects are believed to be small.

Damping Moments and Flutter Characteristics

The variation of aerodynamic damping-moment derivative $C_{h\delta, \omega}$ with oscillating amplitude and Mach number along with associated flutter characteristics is shown in figure 10 for the $c_b/c_a = 0.35$ control at $\alpha = 0^\circ$, and in figures 11 and 12 for the $c_b/c_a = 1.00$ control at $\alpha = 0^\circ$ and 6° , respectively. Data are presented in the different parts of these figures for the various reduced frequencies of the controls tested. These plots of $C_{h\delta, \omega}$ with oscillating amplitude (figs. 10 to 12) present an equivalent linear viscous damping derivative for the system when it is oscillating over a complete cycle at the various amplitudes.

$c_b/c_a = 0.35$ control.- Aerodynamic results for the $c_b/c_a = 0.35$ control (fig. 10) show that the damping was stable for all amplitudes and reduced frequencies tested at Mach numbers from 0.60 to about 0.90 and was generally unstable in the Mach number range from about 0.92 to 1.01, the maximum Mach number tested. The damping derivative $C_{h\delta, \omega}$ was generally fairly constant to maximum test oscillating amplitudes of about 10° at the lower test Mach numbers ($M = 0.6$ to 0.8) and became less stable with increasing amplitude at the intermediate test Mach numbers ($M = 0.85$ to 0.92) such that the aerodynamic damping became slightly unstable for some high test oscillating conditions. At the higher test Mach numbers ($M = 0.94$ to 1.01) maximum unstable values of $C_{h\delta, \omega}$ generally occurred at the low oscillating amplitudes with unstable values of $C_{h\delta, \omega}$ decreasing with an increase in oscillating amplitude, thus leading to the limited amplitude type of flutter response obtained. For this control, $c_b/c_a = 0.35$, changes in test oscillation amplitude did not change the general variation in $C_{h\delta, \omega}$ with Mach number.

When comparing the flutter characteristics with the aerodynamic damping values (fig. 10), it should be remembered that the control system had a certain level of nonaerodynamic damping. Flutter was a self-excited oscillation involving only the degree of freedom of control rotation about the hinge line. In all cases tested for this control, flutter was self-starting (see section entitled "Symbols") and built up in amplitude until a steady-state condition was reached, wherein the aerodynamic energy fed into the oscillation over a complete cycle was equal to the energy dissipated by nonaerodynamic damping (see fig. 7(c)). The flutter frequencies and amplitudes given are for the steady-state oscillatory conditions of this model.

In the Mach number region where the aerodynamic damping was stable, variation within the test reduced-frequency range had little effect on the magnitude of $C_{h\delta, \omega}$ (see figs. 10 and 18). For the region where the aerodynamic damping was unstable, the damping derivative $C_{h\delta, \omega}$ generally became more unstable as the test reduced frequency was decreased and for this model the flutter amplitude also increased with the decrease in reduced frequency.

$c_b/c_a = 1.00$ control.- The variation of $C_{h\delta, \omega}$ with oscillating amplitude for the $c_b/c_a = 1.00$ control was very nonlinear for the complete Mach number and reduced-frequency range tested at both $\alpha = 0^\circ$ and $\alpha = 6^\circ$ (figs. 11 and 12). As such, the variation in $C_{h\delta, \omega}$ with Mach number can be markedly changed depending on the oscillating amplitude in question. This pronounced effect of oscillation amplitude on the damping results might have been expected in view of the extreme nonlinearities in the variation of static hinge moment with deflection angle for a flap-type control with the hinge line located this far rearward. (See ref. 3.) At the low test oscillating amplitudes, $C_{h\delta, \omega}$ was essentially constant at a relatively low level of stable damping for Mach numbers from 0.40 to 0.70 and increased to a very high level of stable damping near $M = 0.88$ (figs. 11 and 12). The damping derivative $C_{h\delta, \omega}$ at $M = 0.88$ was several times larger than the values below $M = 0.70$. Above $M = 0.88$ (at low amplitudes), there was a rapid reduction in aerodynamic damping with increasing Mach number and $C_{h\delta, \omega}$ was unstable from $M \approx 0.95$ to $M = 1.01$, the maximum for these tests. For this hinge-line position, $C_{h\delta, \omega}$ generally became less stable with increasing amplitude at the lower test Mach numbers and more stable at the higher test Mach numbers. Therefore, at the higher test oscillating amplitudes, $C_{h\delta, \omega}$ was unstable at low test Mach numbers and stable at high test Mach numbers, just the opposite of the variation of $C_{h\delta, \omega}$ with Mach number at low amplitudes (figs. 11 and 12). A possible explanation for this high amplitude, low Mach number instability is associated with the phenomenon of stall flutter. Support for this belief can be seen by examining the variation of static hinge moment with deflection for this control shown in figure 9. For Mach numbers from 0.60 to 0.90, there are abrupt breaks in the variation of C_h with δ in the deflection range from 5° to 10° . This type of static variation of moment with deflection can, for the oscillating case, lead to an aerodynamic hysteresis or stall-flutter type of self-excited instability. Examination of figures 11 and 12 shows that the aerodynamic damping of the control is generally reduced and under certain conditions becomes unstable if the control is oscillating at an amplitude which includes these static breaks.

Flutter for the $c_b/c_a = 1.00$ control was also a one-degree-of-freedom, self-excited oscillation and the flutter frequencies and amplitudes given in figures 11 and 12 are again the steady-state oscillatory conditions for this model. Flutter which occurred in the Mach number range from 0.40 to 0.80 was a "bumped" flutter in that, to initiate the instability, the control had to be displaced to some intermediate amplitude and suddenly released. Flutter in the Mach number range from 0.94 to 1.01 was self-starting and the flutter amplitude for this transonic instability was greatly reduced by shifting the hinge line rearward as can be seen by comparing the flutter amplitudes of figure 11 with those of figure 10.

For a wind-off natural frequency of 160 cps and an angle of attack of 6° , the unstable aerodynamic damping at transonic speeds was reduced to a point where the nonaerodynamic damping stabilized the system and eliminated the flutter (figs. 11(c) and 12(c)). The effect of angle of attack and/or reduced frequency was not this pronounced for this control at the other test conditions. In general, variation of test reduced frequency and changing the angle of attack from 0° to 6° had small effects on the overall damping moments.

Although it was not actually done for all cases, it was the opinion of the writers that the control-system flutter encountered in these tests could be eliminated by increasing the nonaerodynamic damping until the damping due to rotation of the control system about the hinge line remained stable throughout the test range.

Spring Moments

Static hinge-moment or spring-moment coefficients are shown in figures 8 and 9 for the two controls tested. These data indicate that the tip store generally had little effect on the static hinge moments. The $c_b/c_a = 0.35$ control (fig. 8, $\alpha = 0^\circ$ and 6°) was closely balanced aerodynamically at low deflections, in the Mach number range from 0.60 to 0.90. In this speed range, the variation of C_h with δ was linear at the lower deflections ($\delta \approx \pm 5^\circ$) and became more underbalanced at the higher deflections. In the Mach number range from 0.95 to the maximum for these tests (1.02), C_h was linear over the complete test range of δ and the aerodynamic-loading center shifted rearward so that the control was considerably underbalanced. With the control hinge line shifted to the midchord position ($c_b/c_a = 1.00$, fig. 9, $\alpha = 0^\circ$) the control was overbalanced or statically unstable for the complete test speed and deflection range. This is generally an undesirable aerodynamic feature; however, the oscillating hinge moments for this control were considered of interest because of the beneficial influence on damping shown by

potential theory for rearward located hinge axes. In the Mach number range from 0.60 to 0.90 there are abrupt breaks in the curves of C_h plotted against δ which are typical of flap-type controls having the hinge line this far rearward. (See, for example, ref. 3.) These extreme nonlinearities are alleviated somewhat by the rearward shift in aerodynamic loading in the test speed range above $M = 0.90$.

The oscillating aerodynamic spring-moment derivatives $C_{h\delta,\omega}$ obtained in this investigation are shown in figures 13 and 14. The reduced frequency for each data point on these figures is given on the corresponding damping curves in figures 10 to 12. Since frequency could not be accurately determined from a few oscillation cycles and since oscillation amplitude changes within each cycle for all but the steady-state flutter conditions, any nonlinear variation of aerodynamic spring-moment parameter with oscillation amplitude could not be determined by the test technique used. Therefore the $C_{h\delta,\omega}$ values given were averaged over some arbitrary oscillating amplitude range. When possible this oscillation amplitude range was chosen to be the same as the linear range over which static $C_{h\delta}$ values were measured. However, for the highly damped oscillatory conditions this was not feasible and the complete amplitude range was used. Therefore, some difference in effective amplitude range exists for the static and oscillatory data comparison shown in figure 15.

The oscillation spring-moment derivative $C_{h\delta,\omega}$ varies with Mach number in much the same manner as the static derivative $C_{h\delta}$ and for the test conditions of these data, static hinge-moment data could be used to make fairly accurate frequency estimates for single-degree-of-freedom transonic control-surface flutter. The aerodynamic balancing effect of shifting the hinge line rearward is clearly shown in figure 15 for the test Mach number range and the effect is about the same for both the static and dynamic aerodynamic stiffness parameters.

In general, changing the angle of attack from 0° to 6° and the variations within the test reduced-frequency range had little effect on the aerodynamic spring-moment parameter $C_{h\delta,\omega}$.

Effect of Hinge-Line Position and Comparison With Theory

The effects of hinge-line position on the oscillating hinge-moment parameters, based on results reported herein and results for the $c_b/c_a = 0.20$ control reported in reference 1, are shown in figures 16 to 20. In figure 16 the variation of aerodynamic stiffness and damping parameters with hinge-line position is shown for representative Mach numbers. These data were arbitrary for a particular control-system

oscillation condition ($\delta_1 \approx \pm 1^\circ$, $f_o \approx 175$) and show typical effects although the results are dependent on the conditions chosen especially with regards to oscillation amplitude. Also shown in figure 16 is an auxiliary abscissa scale for convenience in converting c_b/c_a values to hinge-line location in percent total control chord from the control leading edge. The aerodynamic balancing effect on $C_{h\delta, \omega}$ of shifting the hinge line rearward is shown and this effect is smaller at sonic speed than at the lower test speeds due to the rearward shift in aerodynamic center of pressure associated with supersonic flow. Figure 16 also shows that the control aerodynamic damping is affected considerably more by Mach number than by hinge-line position and the damping is unstable at sonic speeds for the range of hinge-line positions tested at low oscillation amplitudes.

Figures 17 and 18 compare experimental data obtained at $M = 0.60$ with results computed by the two-dimensional incompressible theory of reference 7. The linear theory would be of interest at low oscillation amplitudes and the differences caused by finite airfoil thickness in the experimental case should be relatively small for the thin wing investigated. In computing results from reference 7, a mean camber-line parameter of 0.25 times the overhang length was used, as suggested, to physically represent the local flow at the nose of the control. The choice of this parameter can have a large effect on the magnitude of the computed spring-moment parameters. Therefore better quantitative agreement between experimental and calculated spring moments could possibly be expected if sufficient information were available to establish the proper choice of mean camber-line parameter for the various overhangs. The parameter $kC_{h\delta, \omega}$ was used to represent the aerodynamic damping since, as shown by equation 1, this results in representative numerical values for the spring- and damping-moment components. The data in figure 17 show the variation of hinge-moment parameters for a range of control reduced frequencies and figure 18 is a cross plot of these data to show the variation with hinge-line position. Very good agreement is obtained between experiment and theory for the damping results and good qualitative agreement is obtained for the spring results. The lack of quantitative agreement for the spring-moment parameters can be attributed to uncertainties in the analytical treatment of the local flow at the nose of the control (theory does not permit flow through the gap) as well as aspect ratio and Mach number effects. The effect of Mach number is especially pronounced for the $c_b/c_a = 1.00$ control as shown in figure 12. The very good agreement obtained for the damping parameters is somewhat surprising in view of the existing limitations of the theory. However, the same trends between experiment and theory were obtained at subsonic speeds with the empirically modified two-dimensional compressible theory used for comparison in reference 1. Therefore the indication is that subsonic aerodynamic damping parameters for various hinge-line





positions and low oscillating amplitudes can be estimated reasonably well from available theory. The spring-moment parameters for these same conditions can be computed to a lesser degree of accuracy. The data in figure 17 indicate that, for a given hinge-line position and constant dynamic pressure, increasing the control reduced frequency increases the aerodynamic damping moment but has relatively little effect on the aerodynamic spring moment. The increase in damping moment is approximately proportional to the increase in k which means that $C_{h\delta, \omega}$ remains essentially constant with k for a given control. Figure 18 shows that the aerodynamic balancing effect on the spring-moment derivative of shifting the hinge line rearward is similar for both the static and dynamic case. The stable aerodynamic damping at subsonic speeds is reduced by a rearward movement of the hinge line.

Test results are compared with theory through a Mach number range in figure 19. This comparison is made for the control hinge-line positions tested, and the data are considered applicable only at low oscillating amplitudes. Theoretical values at sonic and supersonic speeds were computed from wing-coefficient expressions given in references 5 and 2. These calculations are permitted under the assumption that at these speeds the control oscillating forces are not influenced by the wing surface in the upstream direction. The qualitative agreement shown in figure 19 is considered good and the transonic experimental data provide a reasonable link between the incompressible and supersonic two-dimensional potential flow theories. This is considered significant since transonic control-surface flutter has been associated with non-potential or separated flow with emphasis placed on shock and boundary-layer interaction (refs. 8, 9, and 10). It has been shown in reference 11, however, that single-degree-of-freedom flutter of a control surface is theoretically possible in potential flow and that the physical parameters necessary for flutter are more likely to be realized at high subsonic or low supersonic speeds than at lower speeds. Therefore, it is believed that the good qualitative agreement between theory and experiment shown here, indicates that dynamic hinge moments even at transonic speeds are strongly dependent on potential flow effects and that for the range of physical parameters tested, theory can serve as a useful guide in predicting the general variation of the control rotation parameters. It must be emphasized, however, that potential and nonpotential flow effects could not be separated in the present tests and the results can certainly be modified by nonpotential factors. The nonlinear aerodynamics shown and the stall flutter at subsonic Mach numbers for the $c_b/c_a = 1.00$ control emphasize the nonpotential flow effects.

Dynamic hinge-moment results for the complete range of parameters tested are summarized in figure 20. Data for these vector diagrams were chosen at oscillation amplitudes and reduced frequencies which would



establish phase angle boundaries that include all of the test data. The symbols locate the end point of the vector representing the resultant aerodynamic hinge moment, and multiple symbols for a particular Mach number indicate extreme values for that Mach number. For the hinge-line positions which gave underbalanced spring moments throughout the speed range ($c_b/c_a = 0.20$ and 0.35), the results show in the unstable damping range a phase angle boundary of about 150° . Since results also show that the oscillating and static aerodynamic spring-moment derivatives are approximately the same, static hinge-moment data at transonic speeds together with this phase angle (150°) would provide a satisfactory empirical representation of the maximum unstable aerodynamic damping moments encountered in this investigation. The phase angle boundaries change radically when the hinge line is moved to the midchord of the control ($c_b/c_a = 1.00$) such that the control becomes aerodynamically overbalanced.

CONCLUSIONS

Oscillating hinge-moment tests at Mach numbers from 0.40 to 1.02 for a flap-type control hinged at three different positions (ratios of balance chord to control chord c_b/c_a of 0.20, 0.35, and 1.00) indicate the following conclusions:

1. Aerodynamic damping derivatives vary considerably with control oscillation amplitude and the nonlinear effects of amplitude were generally larger for the midchord ($c_b/c_a = 1.00$) hinge position.
2. Control aerodynamic damping was unstable for all hinge-line positions tested in the Mach number range from about 0.90 to the maximum speed tested.
3. The damping was generally stable at Mach numbers below 0.90, although it was unstable at subsonic speeds for high oscillation amplitude of the control hinged at midchord.
4. A self-excited flutter involving only rotation of the control about the hinge line was associated with the unstable damping. Flutter amplitude in all cases was self-limiting and, at transonic speeds, the flutter amplitude was decreased by a rearward movement of the hinge line.
5. The aerodynamic spring moments varied from underbalanced to overbalanced for the range of hinge-line positions tested and the oscillating spring-moment derivative ($C_{h\delta, \omega}$) varied with Mach number in much the same manner as the static derivative ($C_{h\delta}$).

6. Changing the angle of attack from 0° to 6° and/or variations within the test reduced-frequency range generally had little effect on the oscillating hinge-moment derivatives $C_{h\delta,\omega}$ and $C_{h\dot{\delta},\omega}$.

7. Existing incompressible theory predicted very well the damping results and to a lesser degree the spring results obtained at low test speeds for the range of hinge positions tested. This theory together with supersonic theory can be used as a guide in predicting the general variation of dynamic hinge-moment parameters with Mach number at transonic speeds for low oscillating amplitudes.

8. The good qualitative agreement between theory and experiment indicates the strong possibility of single-degree-of-freedom flutter of a control surface at transonic speeds even in potential flow; however, the tests also indicate that results can be modified by nonpotential effects.

Langley Aeronautical Laboratory,
National Advisory Committee for Aeronautics,
Langley Field, Va., February 20, 1957.

CONFIDENTIAL

REFERENCES

1. Thompson, Robert F., and Moseley, William C., Jr.: Oscillating Hinge Moments and Flutter Characteristics of a Flap-Type Control Surface on a 4-Percent-Thick Unswept Wing With Low Aspect Ratio at Transonic Speeds. NACA RM L55K17, 1956.
2. Garrick, I. E., and Rubinow, S. I.: Flutter and Oscillating Air-Force Calculations for an Airfoil in a Two-Dimensional Supersonic Flow. NACA Rep. 846, 1946. (Supersedes NACA TN 1158.)
3. Thompson, Robert F.: Hinge-Moment, Lift, and Pitching-Moment Characteristics of a Flap-Type Control Surface Having Various Hinge-Line Locations on a 4-Percent-Thick 60° Delta Wing - Transonic-Bump Method. NACA RM L54B08, 1954.
4. Anon.: Tables of Aerodynamic Coefficients for an Oscillating Wing-Flap System in a Subsonic Compressible Flow. Rep. F.151, Nationaal Luchtvaartlaboratorium, Amsterdam, May 1954.
5. Nelson, Herbert C., and Berman, Julian H.: Calculations on the Forces and Moments for an Oscillating Wing-Aileron Combination in Two-Dimensional Potential Flow at Sonic Speed. NACA Rep. 1128, 1953. (Supersedes NACA TN 2590.)
6. Runyan, Harry L., and Watkins, Charles E.: Considerations on the Effect of Wind-Tunnel Walls on Oscillating Air Forces for Two-Dimensional Subsonic Compressible Flow. NACA Rep. 1150, 1953. (Supersedes NACA TN 2552.)
7. Theodorsen, Theodore, and Garrick, I. E.: Nonstationary Flow About A Wing-Aileron-Tab Combination Including Aerodynamic Balance. NACA Rep. 736, 1942.
8. Erickson, Albert L., and Stephenson, Jack D.: A Suggested Method of Analyzing for Transonic Flutter of Control Surfaces Based on Available Experimental Evidence. NACA RM A7F30, 1947.
9. Biot, M. A., and Arnold, Lee: Investigation of Aileron Compressibility Flutter. Tech. Rep. 6341 (ATI No. 108003), Air Materiel Command, U. S. Air Force, Aug. 1950.
10. Smilg, Benjamin: The Prevention of Aileron Oscillations at Transonic Airspeeds. AAF TR No. 5530, Materiel Command, Army Air Forces, Dec. 24, 1946.
11. Runyan, Harry L.: Effect of Various Parameters Including Mach Number on the Single-Degree-of-Freedom Flutter of a Control Surface in Potential Flow. NACA TN [REDACTED]

TABLE I

TIP-STORE ORDINATES

[Percent of store length]



x	r
0	0
1.95	.95
4.72	2.03
7.51	2.88
10.29	3.52
15.85	4.43
21.40	5.04
26.93	5.49
29.73	5.67
32.53	5.80
35.33	5.84
Straight line	
49.73	5.84
52.53	5.81
55.33	5.76
60.93	5.51
66.40	5.13
72.00	4.63
77.60	4.03
83.20	3.35
88.66	2.63
93.73	1.95
96.00	1.63
98.13	1.28
100.00	0
Trailing-edge radius	0.56

TABLE II

NATURAL FIRST BENDING AND TORSION FREQUENCIES OF WING¹

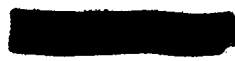
Test condition	Bending, cps	Torsion, cps
Light tip store	120	330
Heavy tip store	67	160

¹The control surface was clamped at 8.2 inches along the hinge line (fig. 5) when measuring these frequencies.

TABLE III

MOMENT OF INERTIA OF CONTROL SYSTEM

Control	I, slug-ft ²	Figures
$c_b/c_a = 0.35$	1.22×10^{-5}	10(a) to 10(d)
$c_b/c_a = 0.35$	4.34	10(e)
$c_b/c_a = 1.00$	1.09	11 and 12



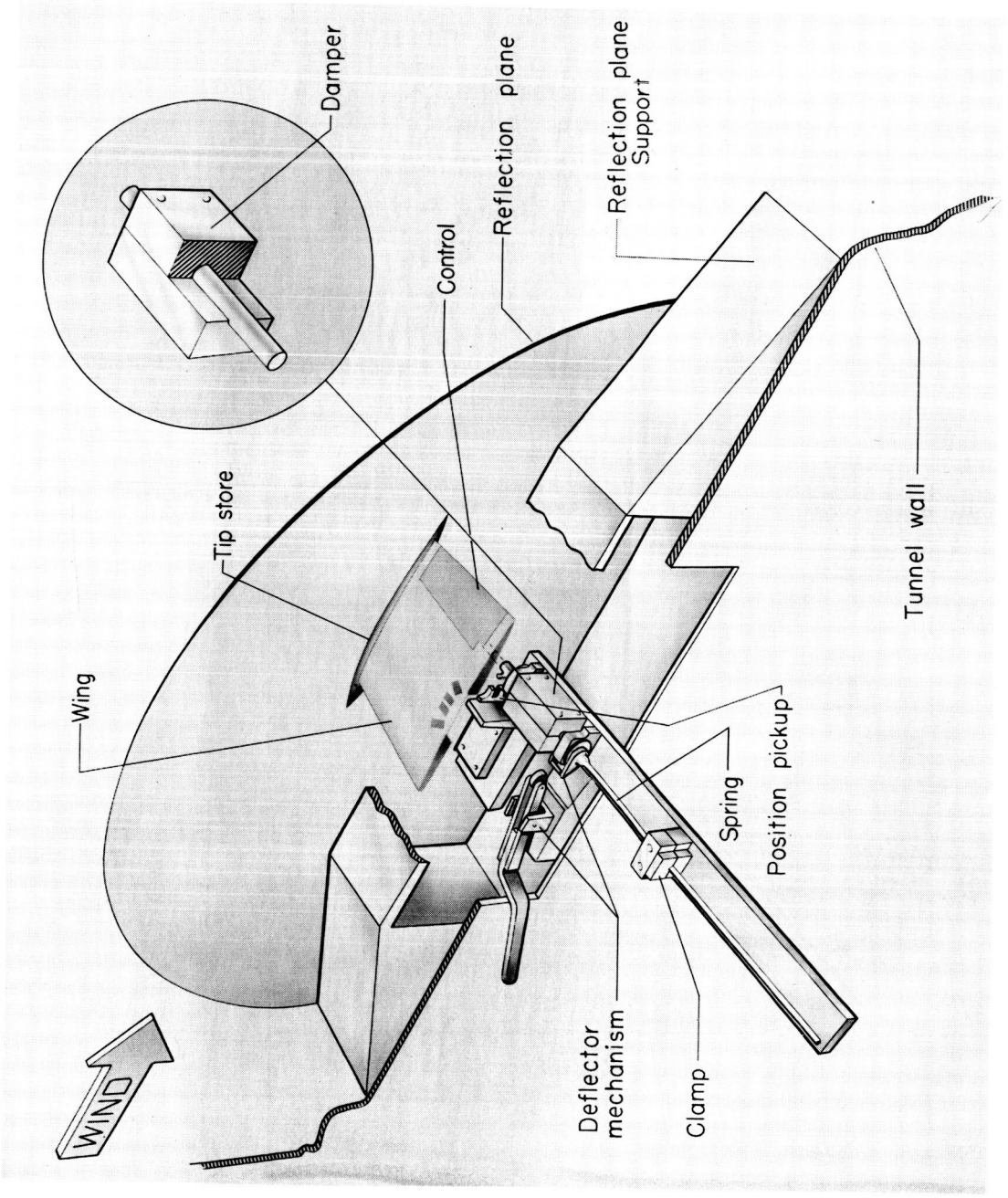
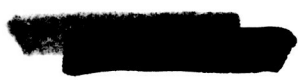


Figure 1.- Schematic drawing of test installation. L-90563.1



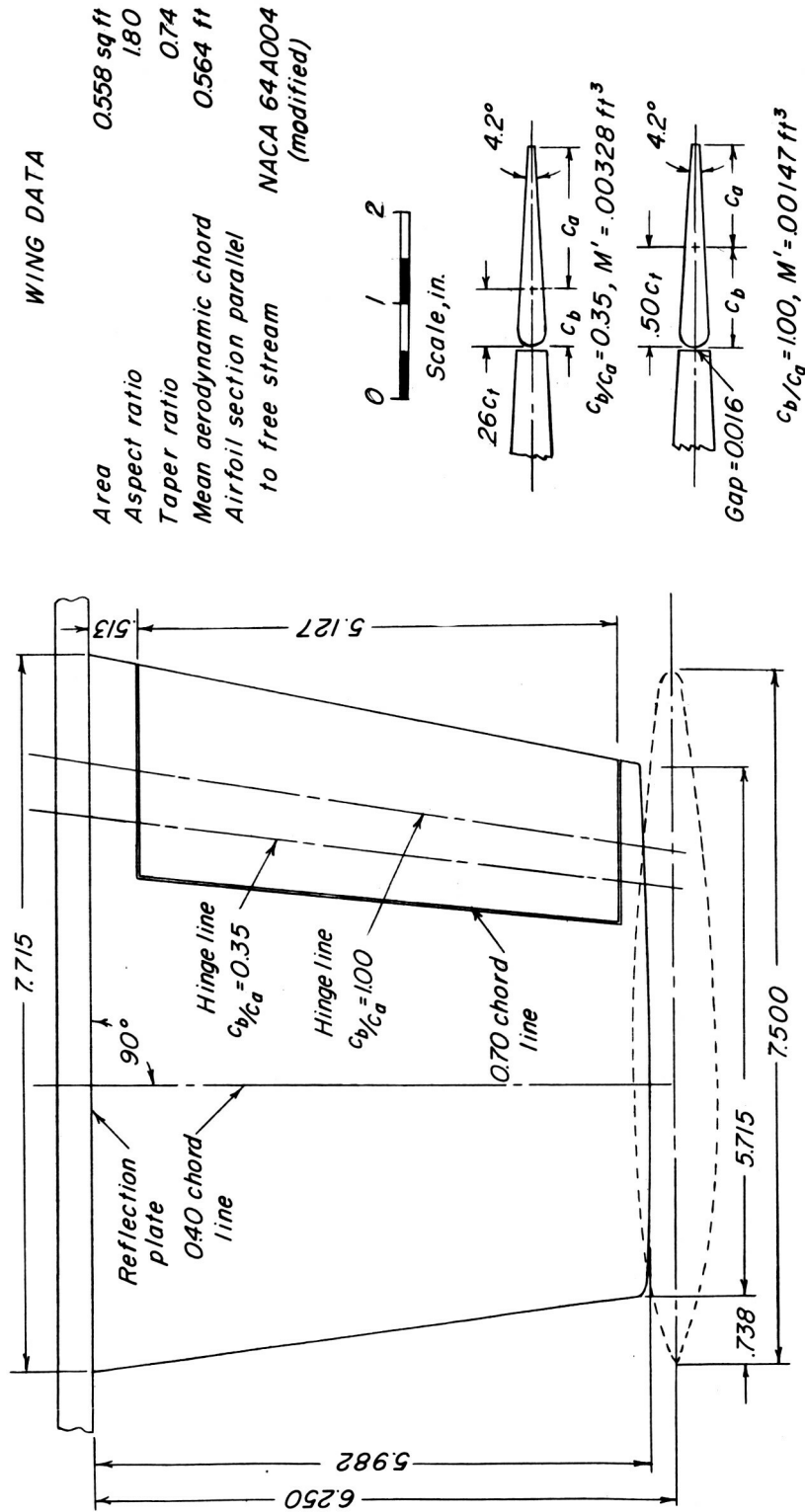
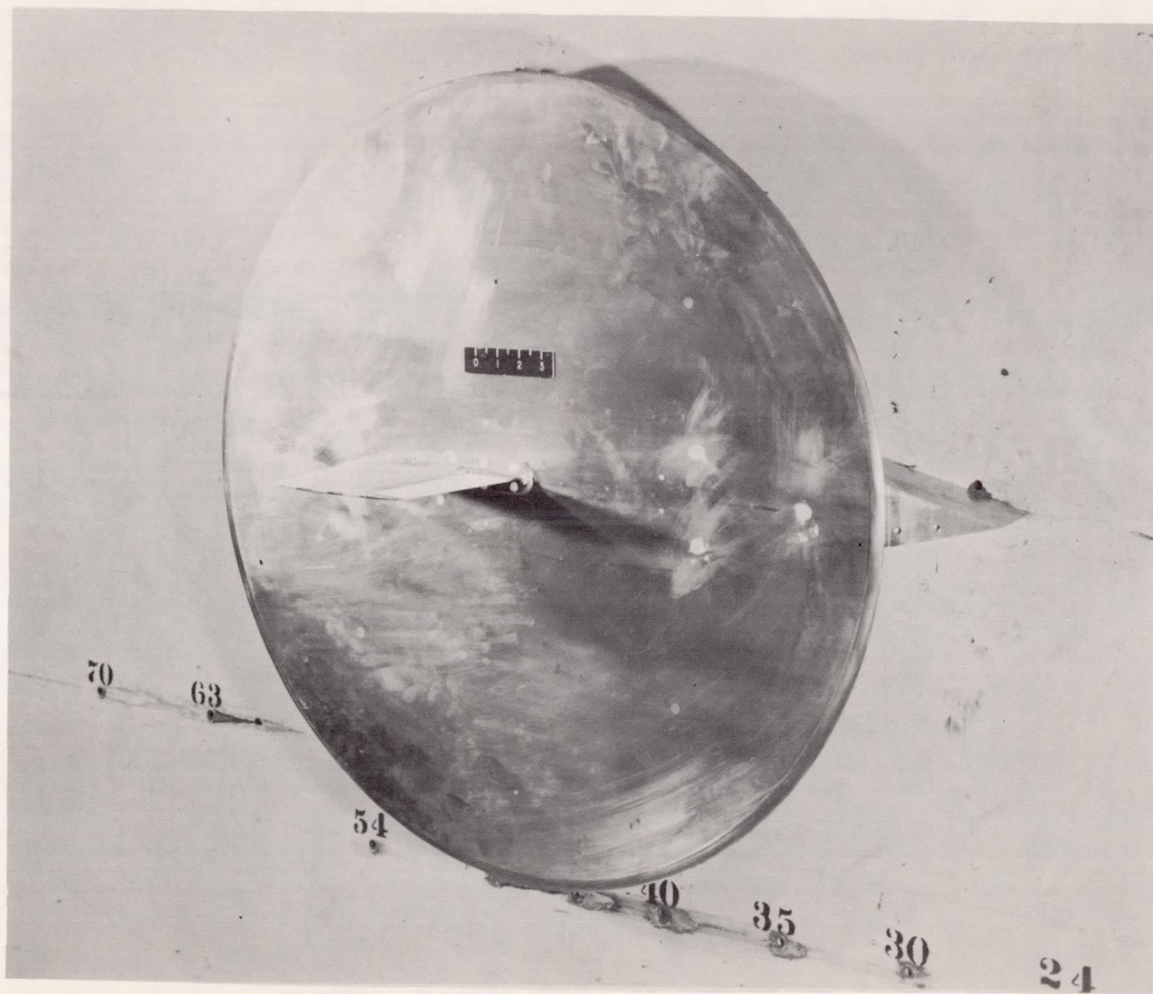


Figure 2.- General dimensions of the test model.

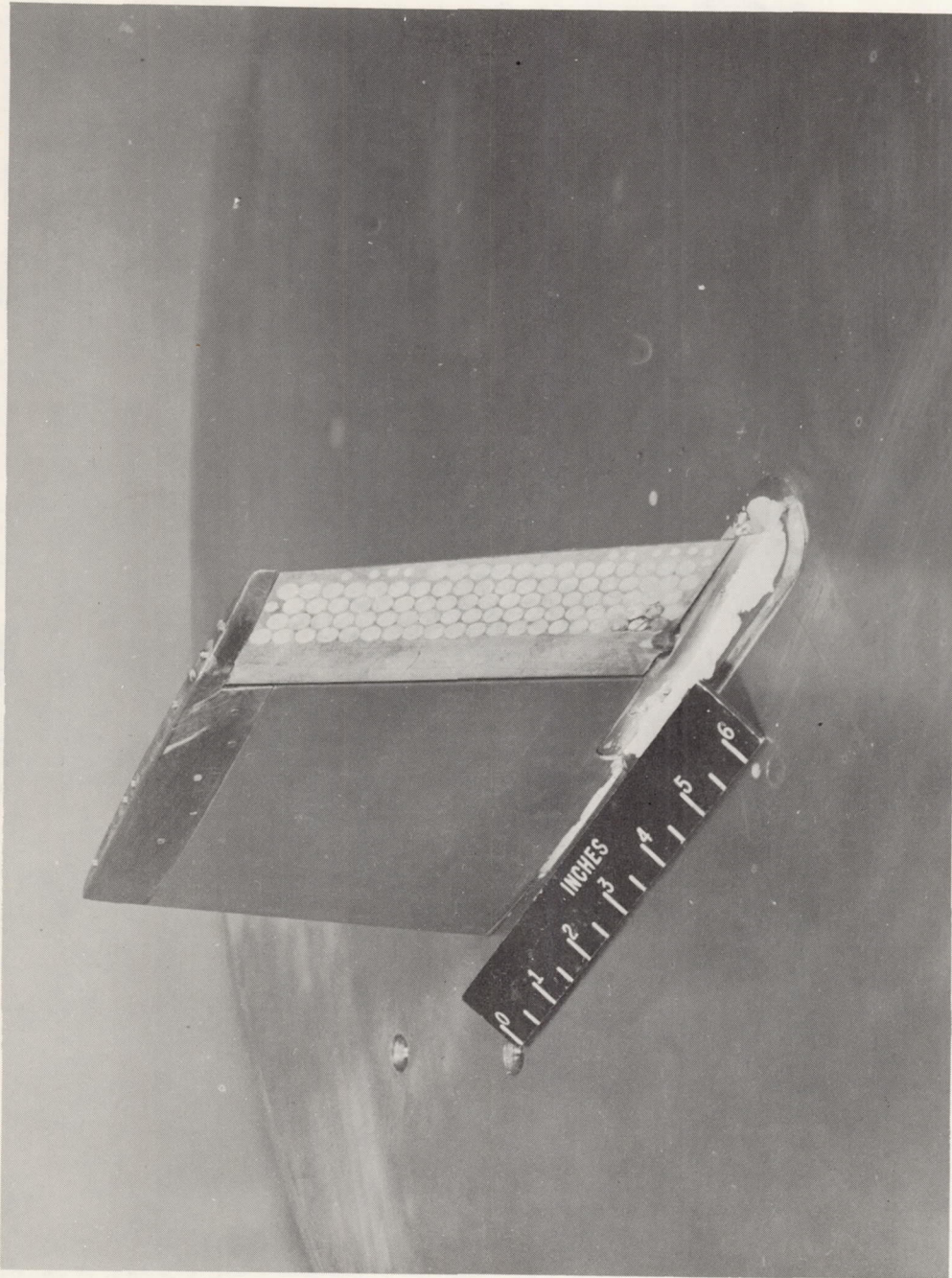
CONFIDENTIAL



(a) Model and reflection plane mounted in tunnel. L-86715

Figure 3.- Photographs of the model.

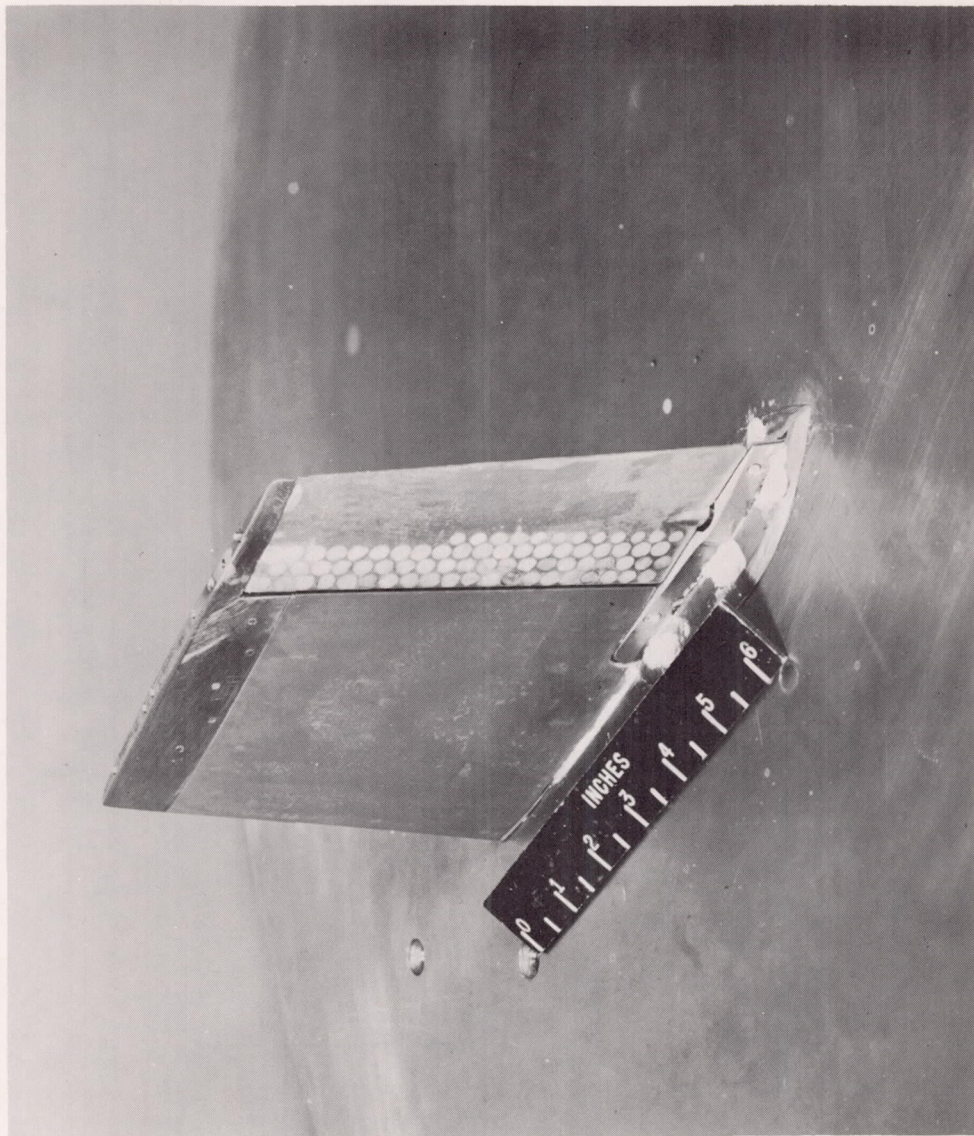
CONFIDENTIAL



L-96429

(b) $c_b/c_a = 0.35$ control.

Figure 3.- Continued.



L-96427

(c) $c_{b/c_a} = 1.00$ control.

Figure 3.- Concluded.

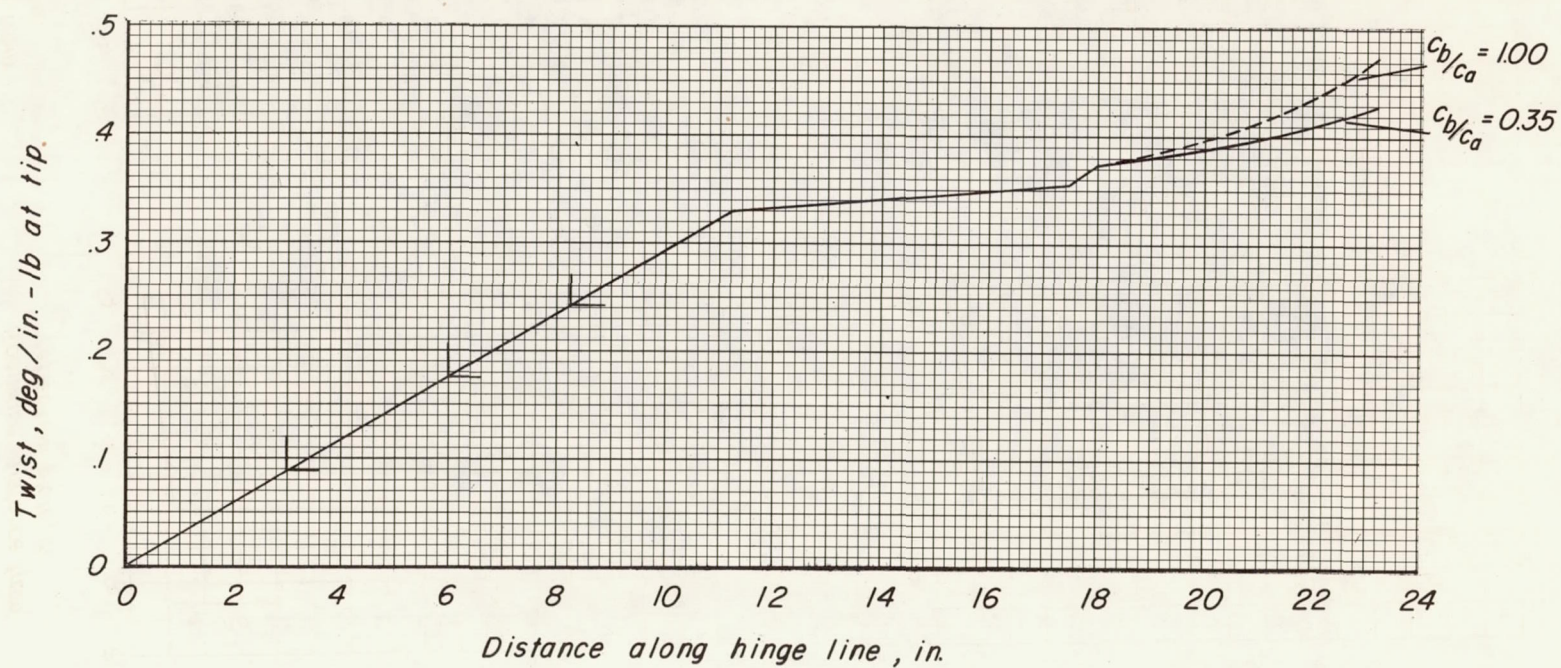
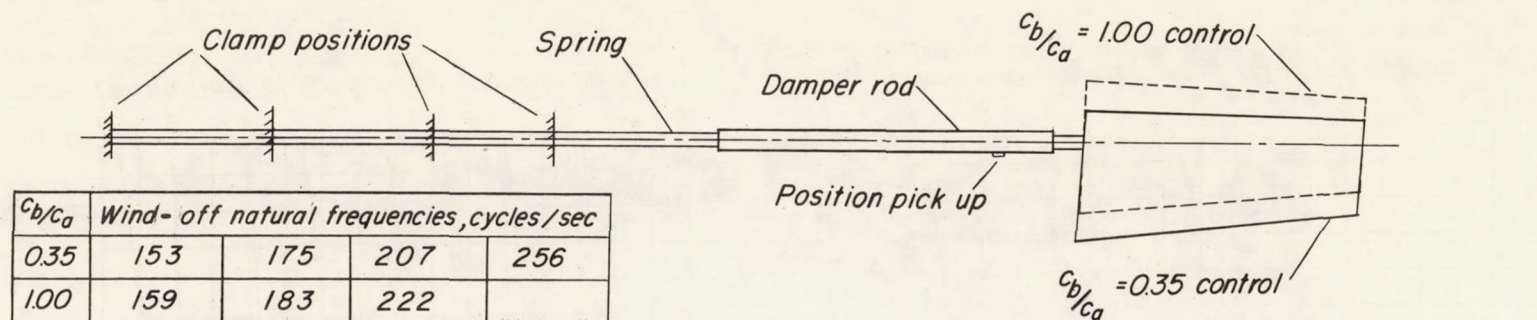


Figure 4.- Frequency and spanwise variation of control system stiffness for various clamp positions.

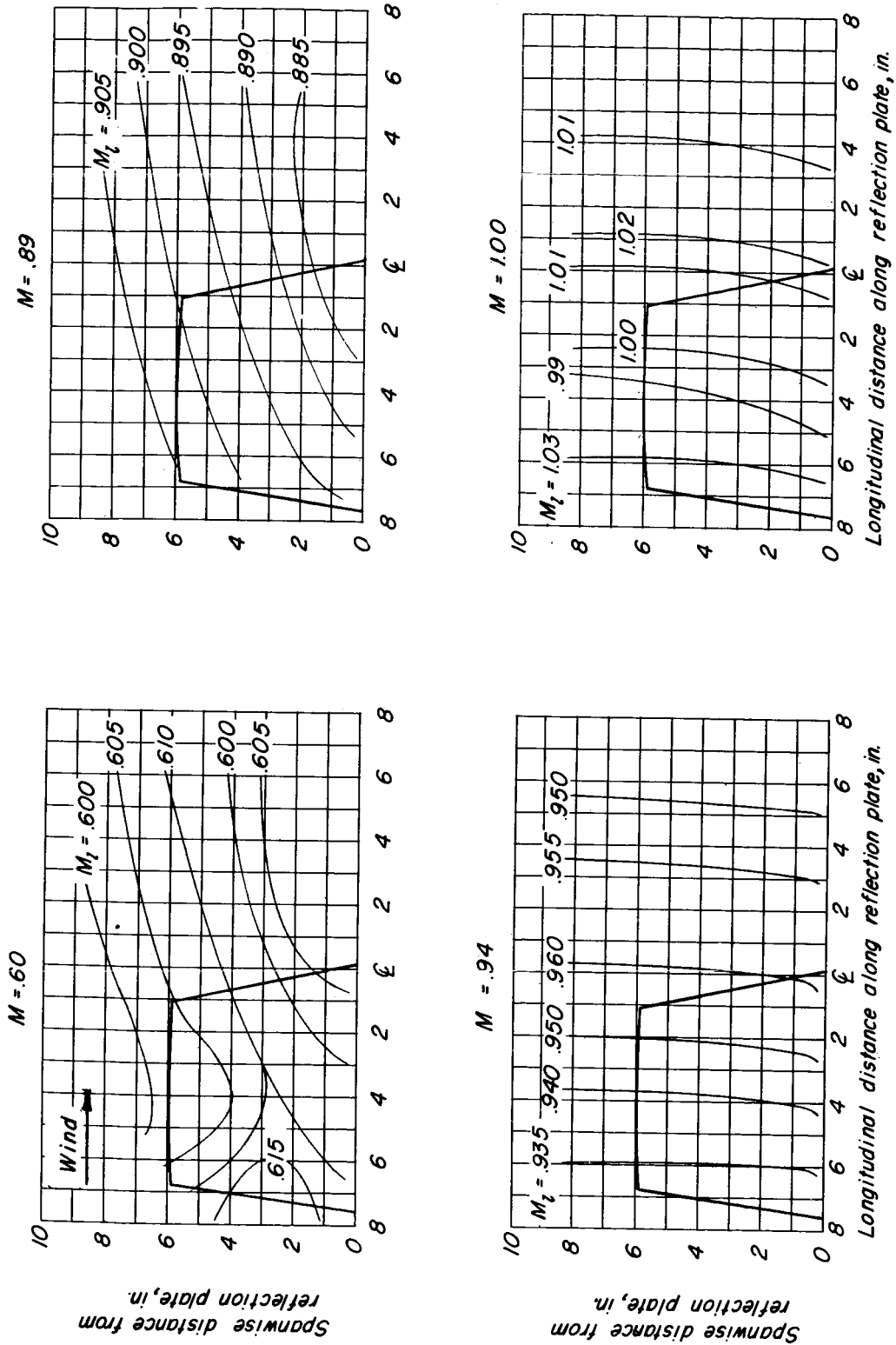


Figure 5.- Typical variation of Mach number contours over the side-wall reflection plate with no model in place.

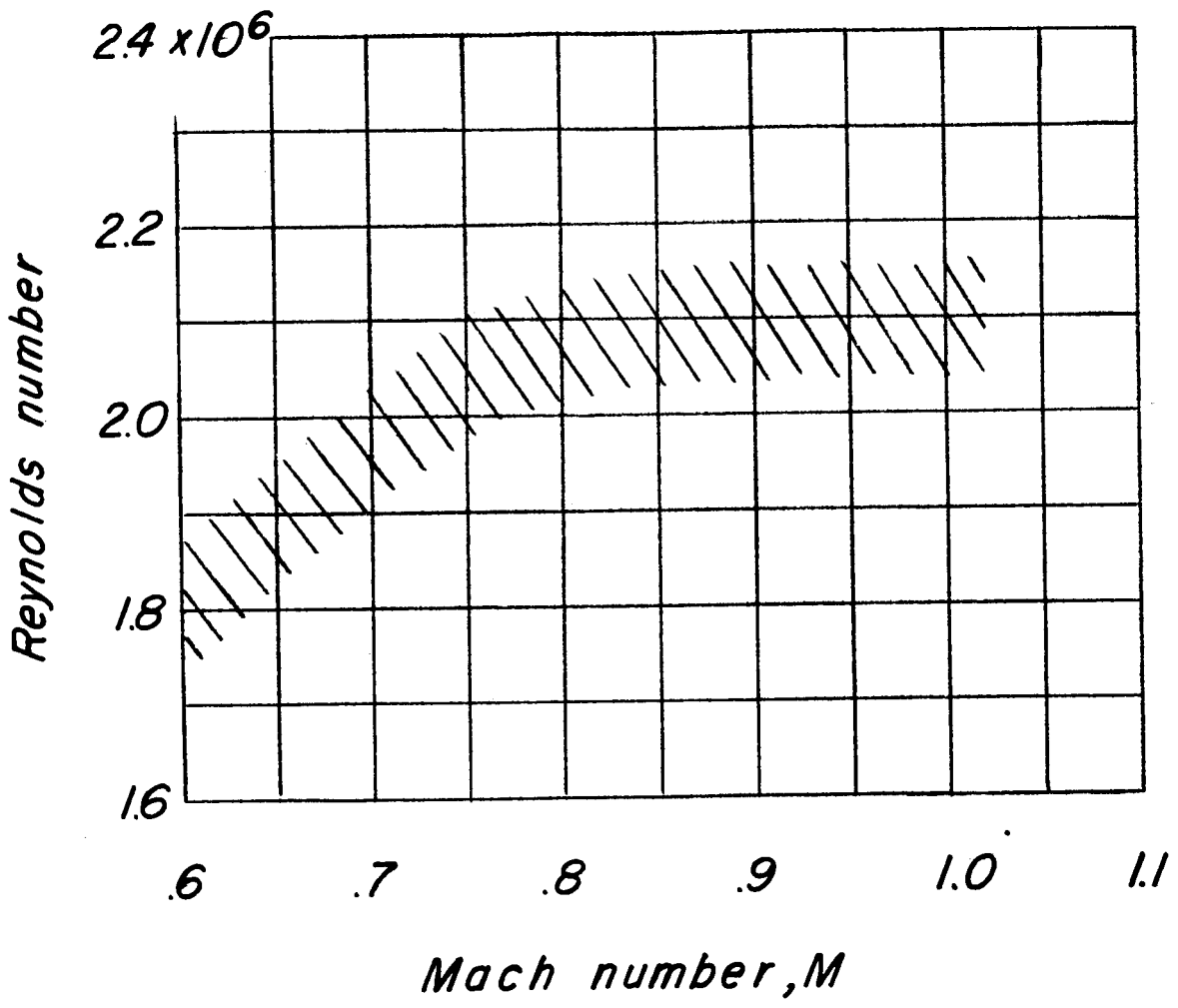
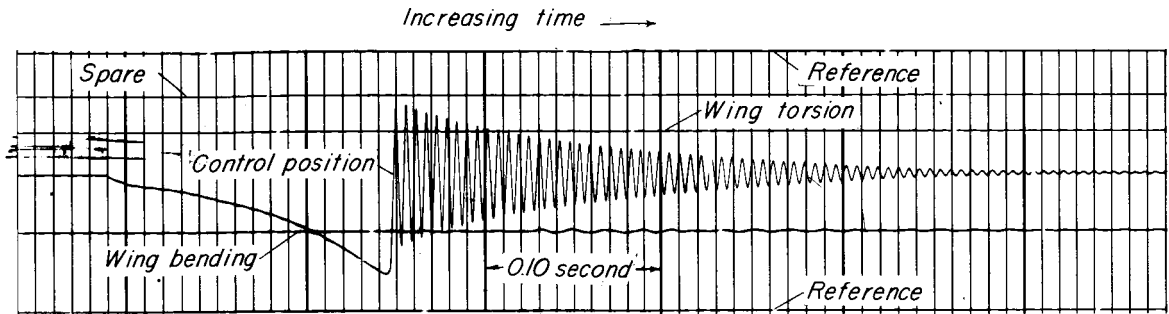
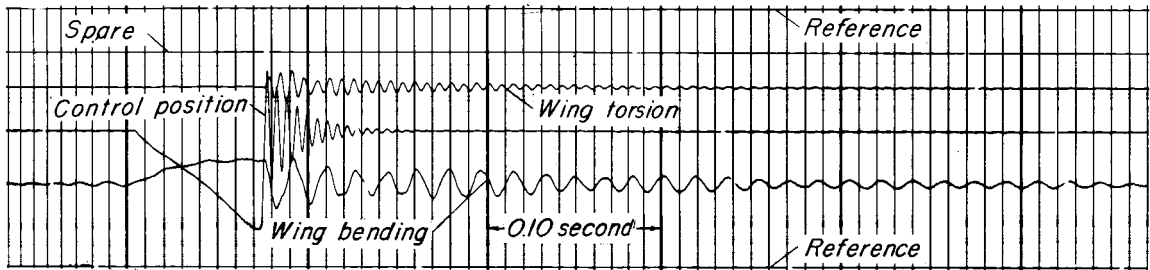


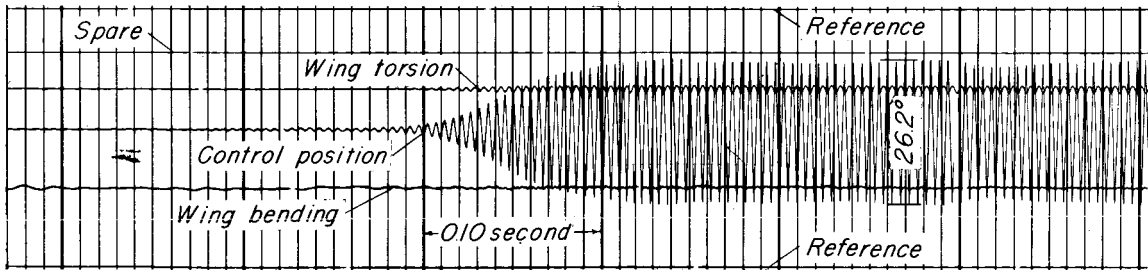
Figure 6.- Variation of test Reynolds number with Mach number.



(a) Wind-off, control released at $\delta=10^\circ$

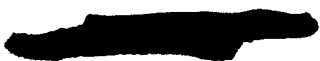


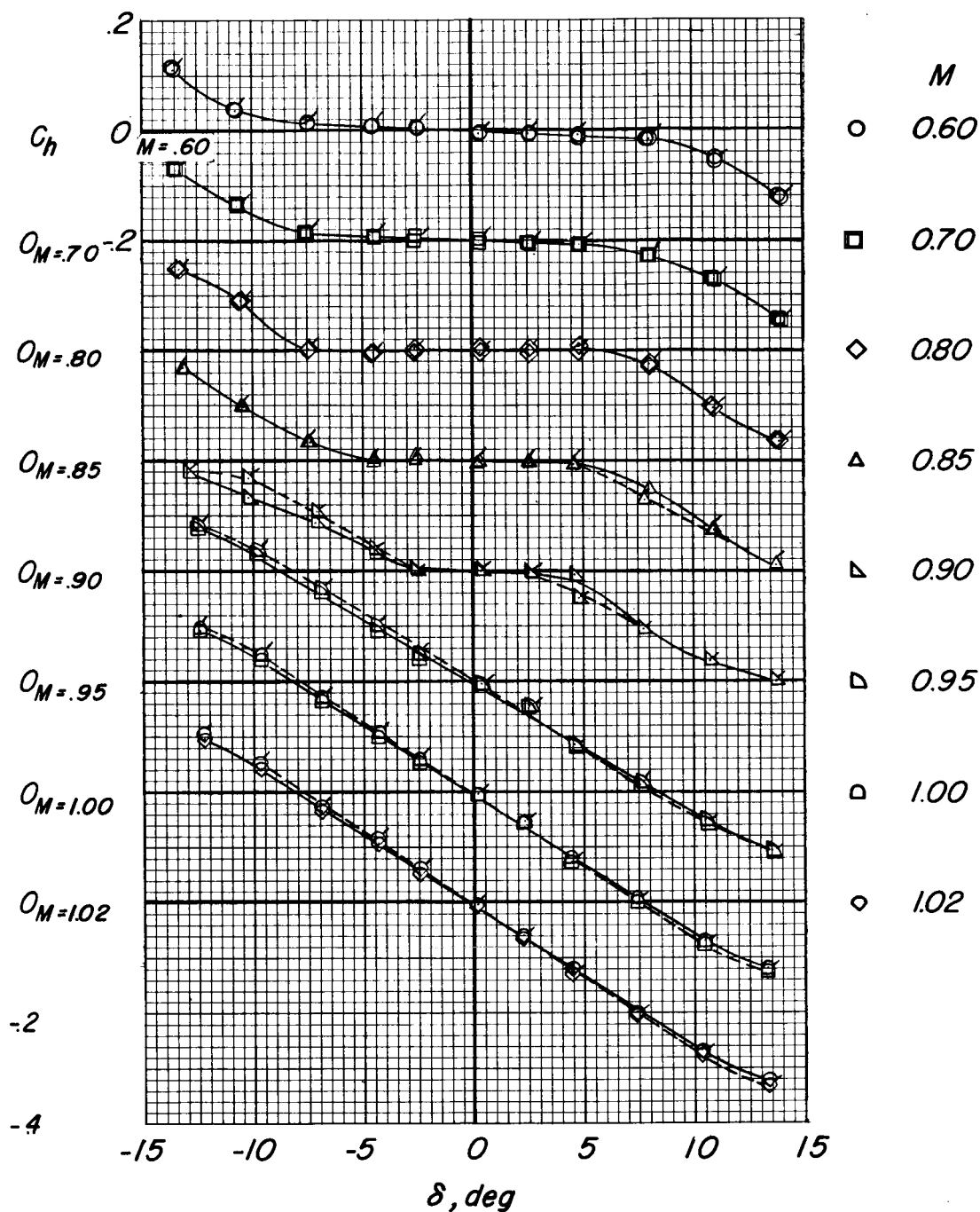
(b) $M=0.70$, control released at $\delta=10^\circ$



(c) $M=1.00$, control released at $\delta=0^\circ$

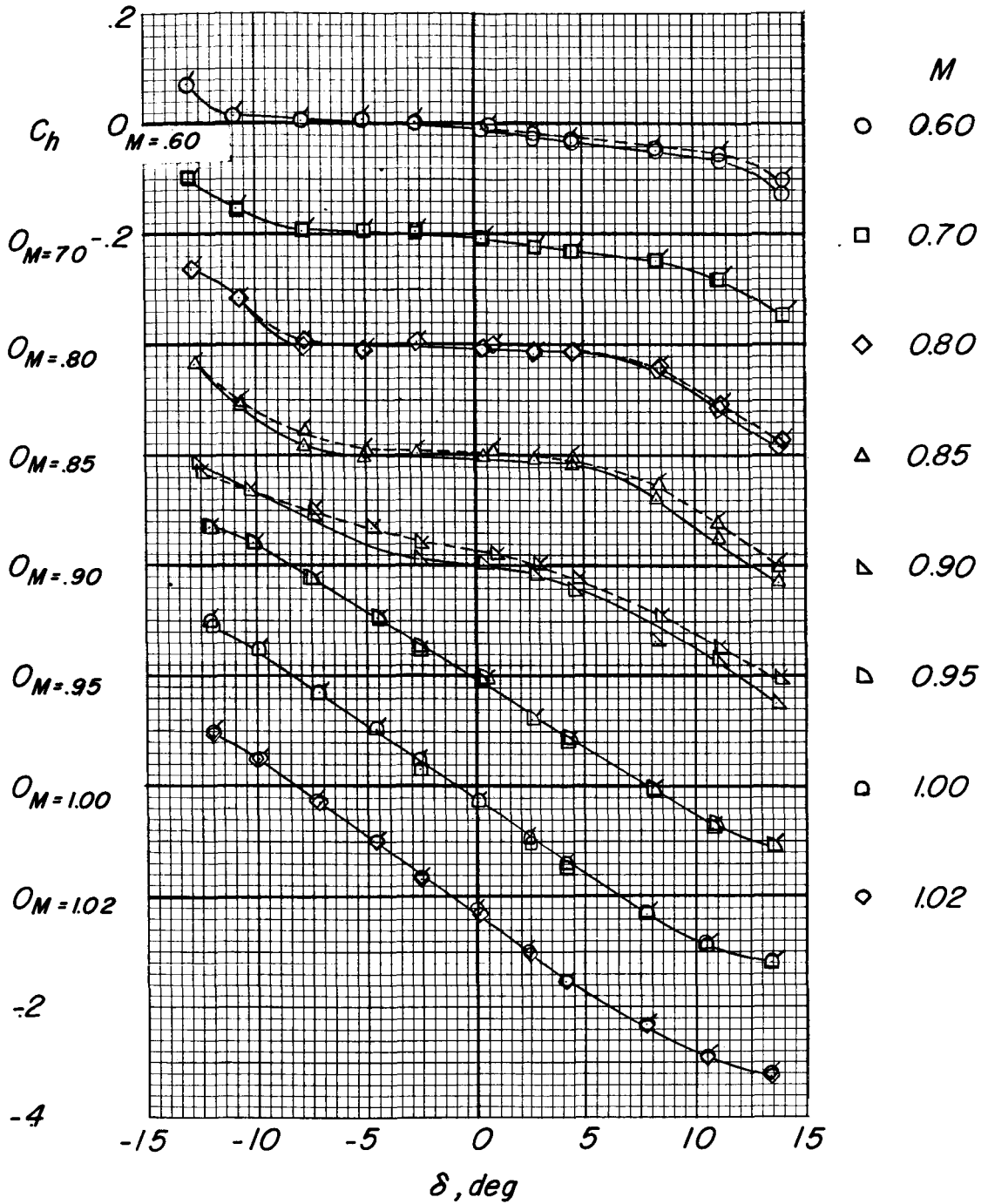
Figure 7.- Typical oscillograph records. Heavy tip store; $\alpha = 0^\circ$; $f_0 = 175$ cps; $c_b/c_a = 0.35$.





(a) $\alpha = 0^\circ$.

Figure 8.- Variation of static hinge-moment coefficient with control deflection for various Mach numbers. Flagged symbols denote tip-store on model; $c_b/c_a = 0.35$.



(b) $\alpha = 6^\circ$.

Figure 8.- Concluded.



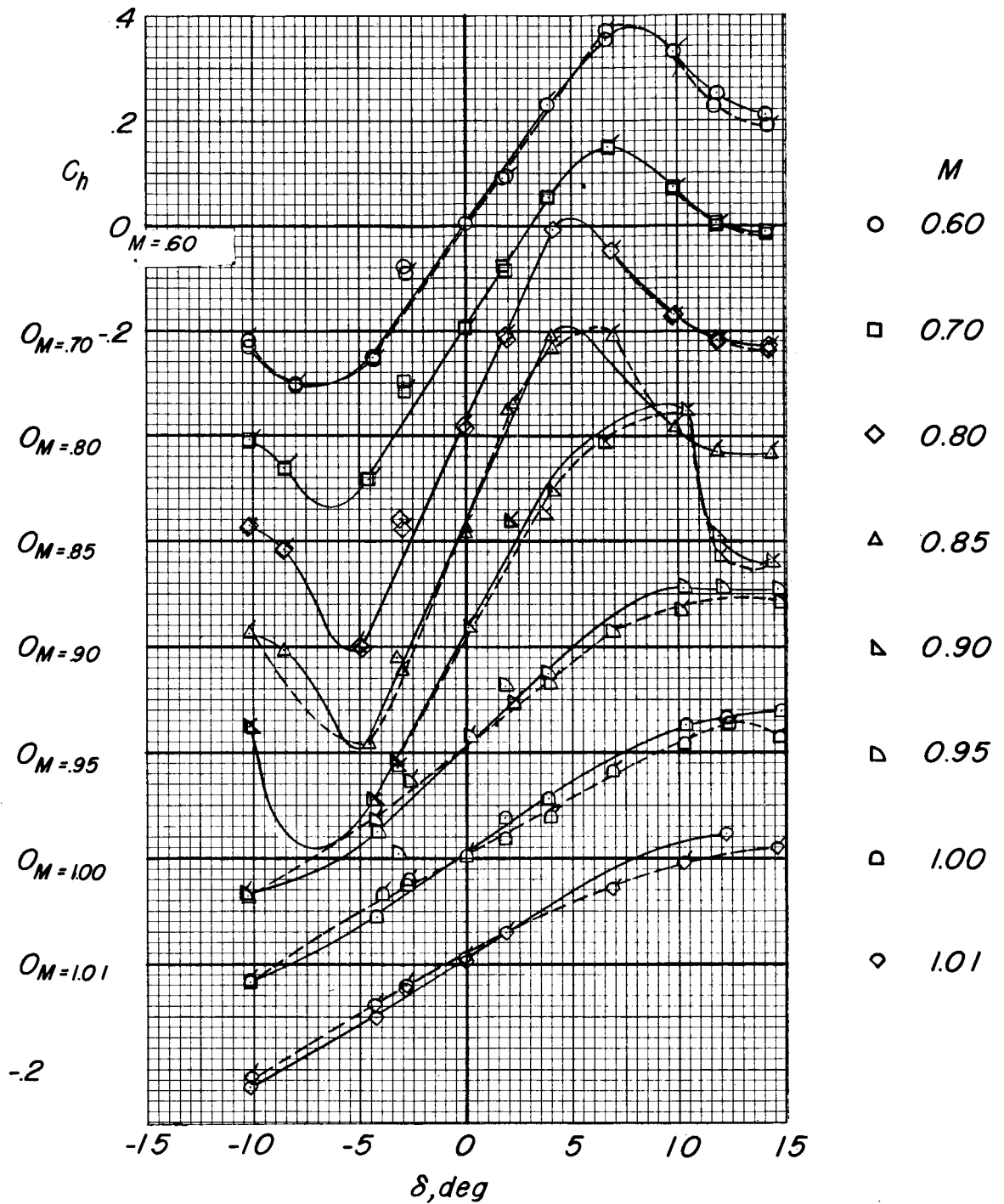
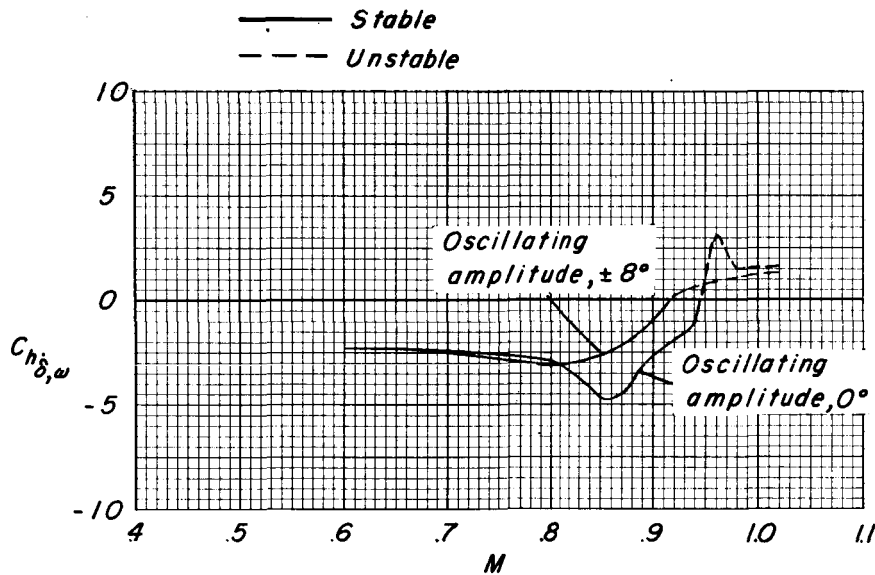
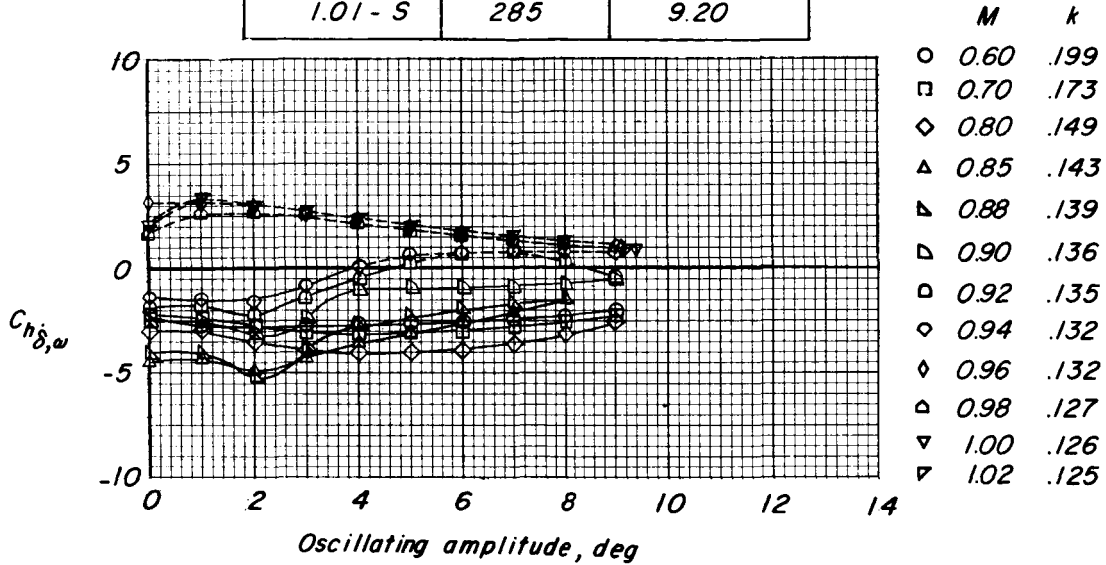


Figure 9.- Variation of static hinge-moment coefficient with control deflection for various Mach numbers. Flagged symbols denote tip-store on model; $c_b/c_a = 1.00$; $\alpha = 0^\circ$.



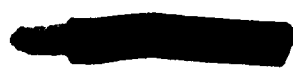
Flutter Characteristics

M	Frequency	Amplitude
0.60 to 0.94	No flutter	
0.96 - S	281	9.05
0.98 - S	278	9.00
1.00 - S	282	9.40
1.01 - S	285	9.20



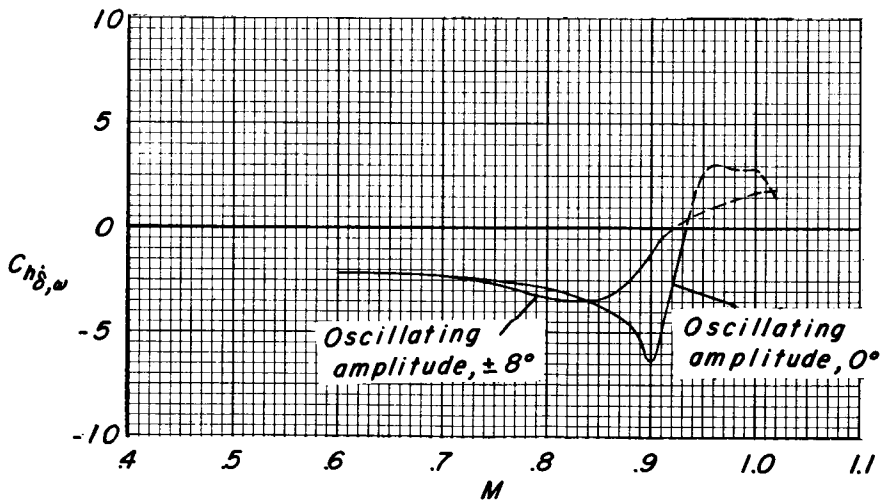
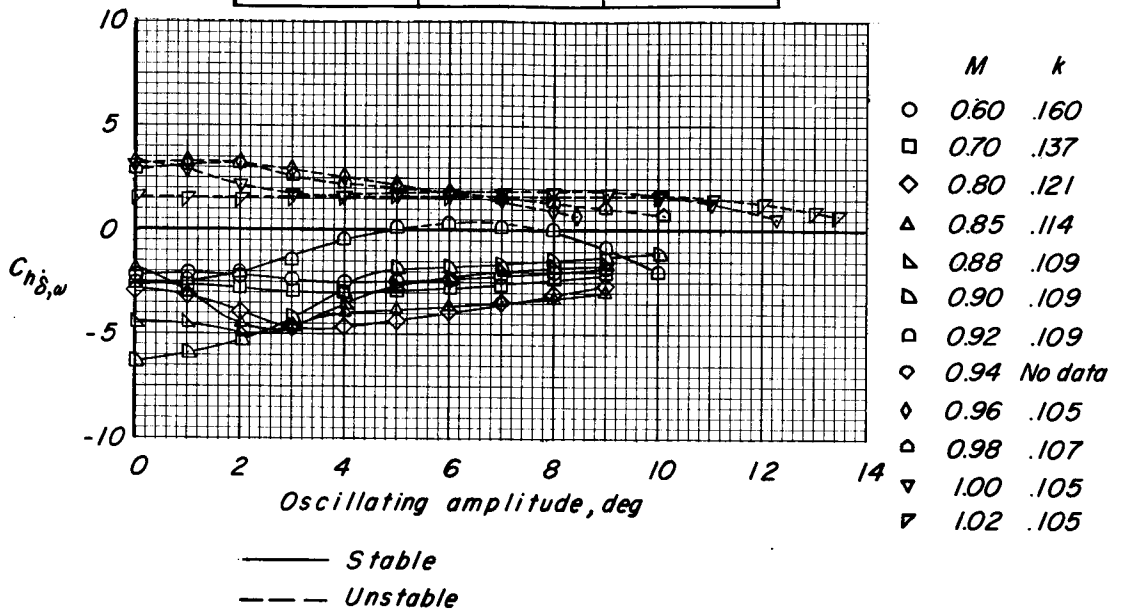
(a) $f_0 = 256$.

Figure 10.- Flutter characteristics and variation of aerodynamic damping derivative with oscillation amplitude for various Mach numbers. $c_b/c_a = 0.35$; $\alpha = 0^\circ$.



Flutter Characteristics

M	Frequency	Amplitude
0.60 to 0.92	No flutter	
0.96 - S	225 cps	8.4°
0.98 - S	235 cps	10.05°
1.00 - S	237 cps	12.2°
1.02 - S	240 cps	13.4°



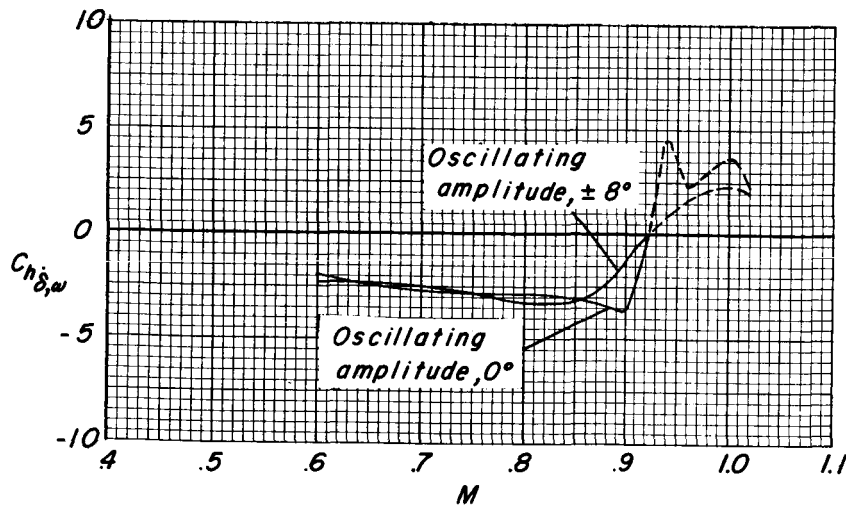
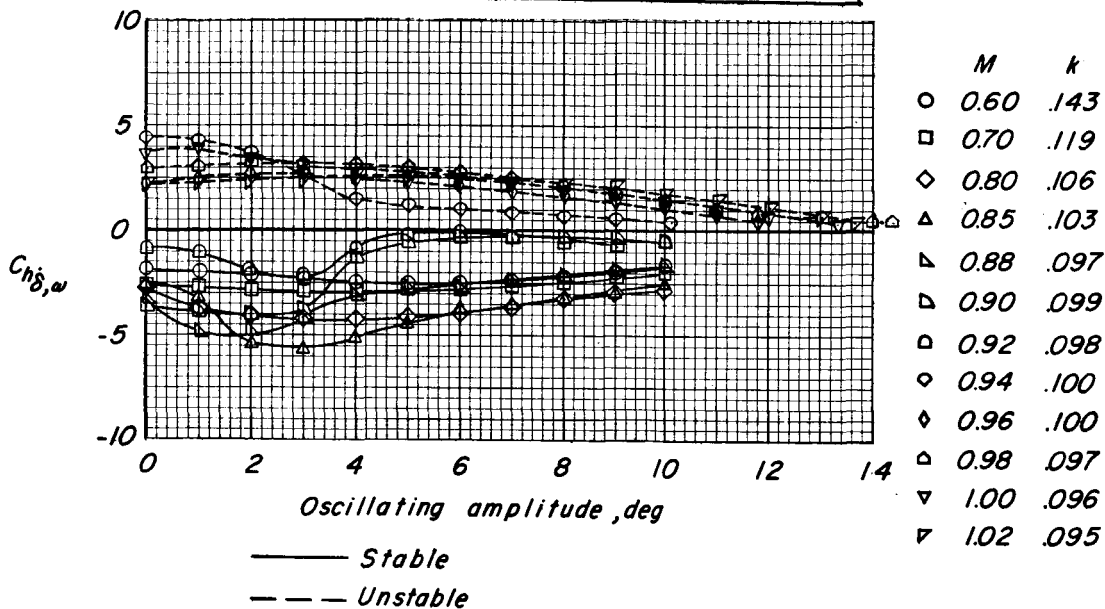
(b) $f_0 = 207$.

Figure 10.- Continued.



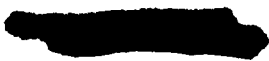
Flutter Characteristics

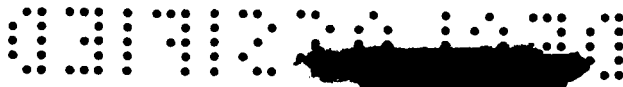
M	Frequency	Amplitude
0.60 to 0.92	No flutter	
0.94 - S	206	10.1
0.96 - S	210	11.75
0.98 - S	208	14.3
1.00 - S	210	13.2
1.02 - S	213	13.6



(c) $f_0 = 175$.

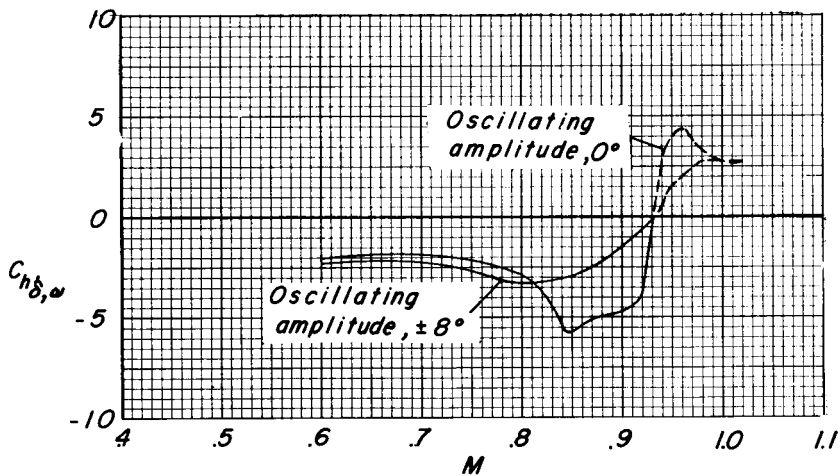
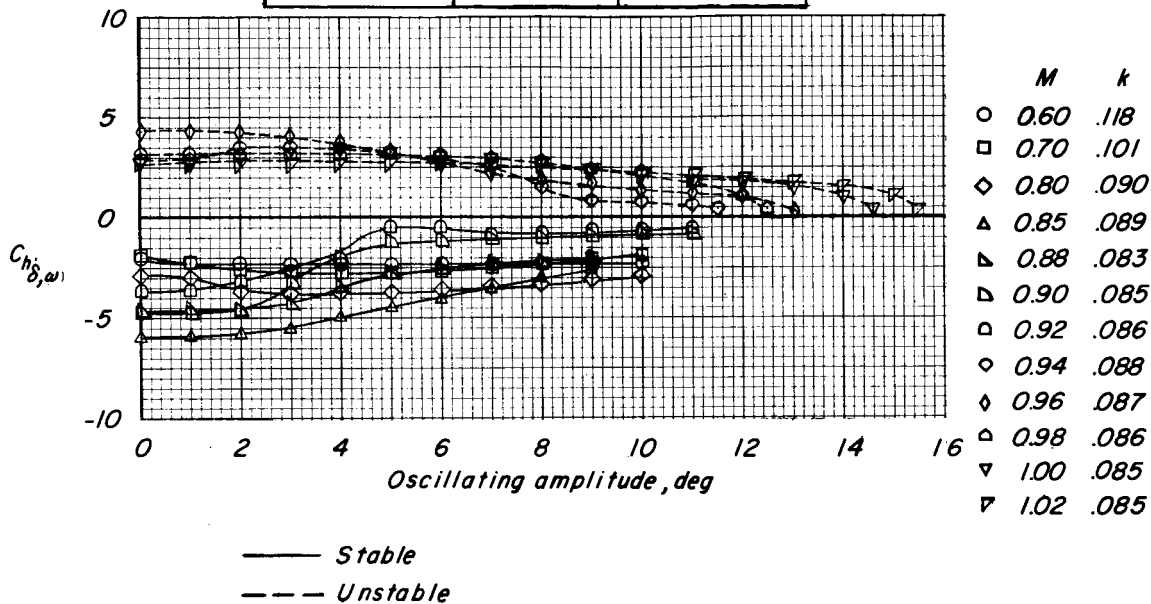
Figure 10.- Continued.





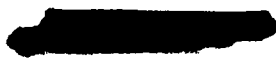
Flutter Characteristics

<i>M</i>	<i>Frequency</i>	<i>Amplitude</i>
0.60 to 0.92	No flutter	
0.94 - S	184 cps	11.5°
0.96 - S	186 cps	13.0°
0.98 - S	189 cps	12.5°
1.00 - S	191 cps	14.6°
1.02 - S	195 cps	15.5°



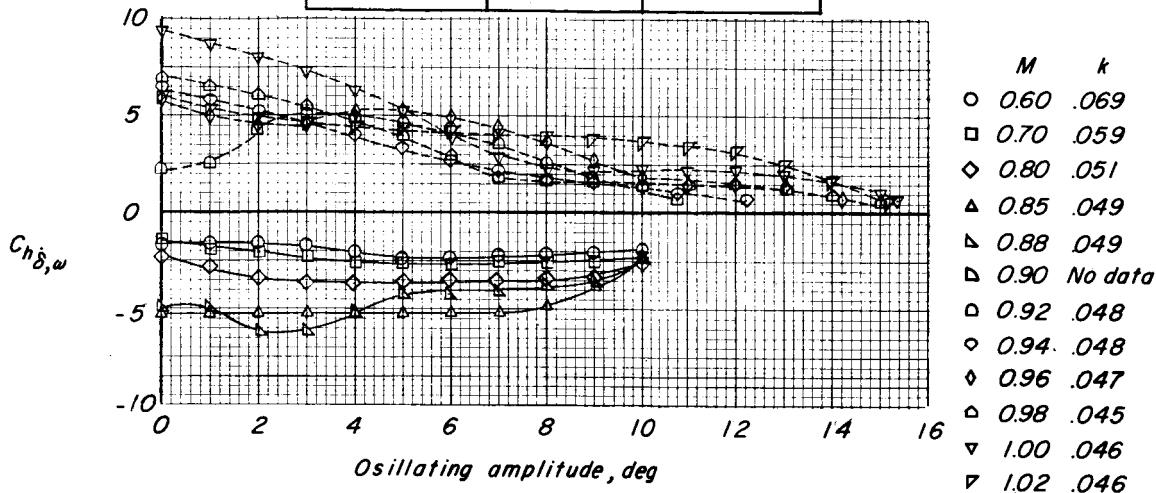
(d) $f_o = 153.$

Figure 10.- Continued.

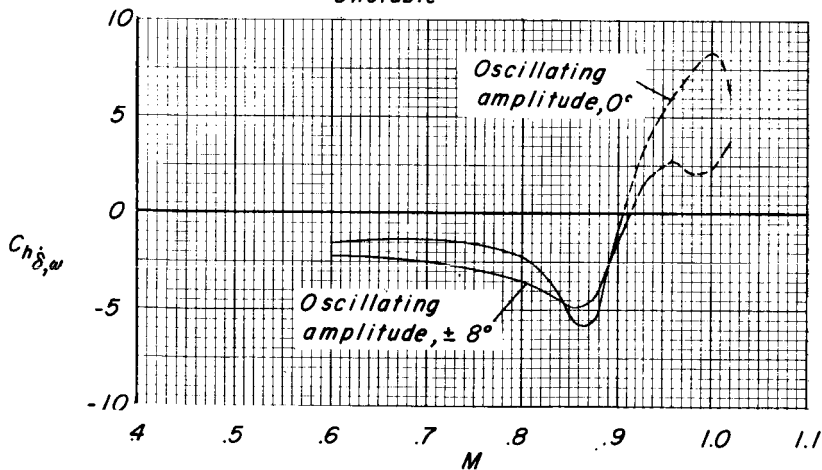


Flutter Characteristics

<i>M</i>	<i>Frequency</i>	<i>Amplitude</i>
<i>No flutter</i>		
0.60 to 0.88		
0.92 - S	97.2 cps	10.75°
0.94 - S	100 cps	12.20°
0.96 - S	100 cps	14.20°
0.98 - S	99 cps	15.0°
1.00 - S	104.2 cps	15.35°
1.02 - S	105.5 cps	15.20°



— Stable
 - - - Unstable



(e) $f_0 = 86.5$; I increased as shown in table III.

Figure 10.- Concluded.



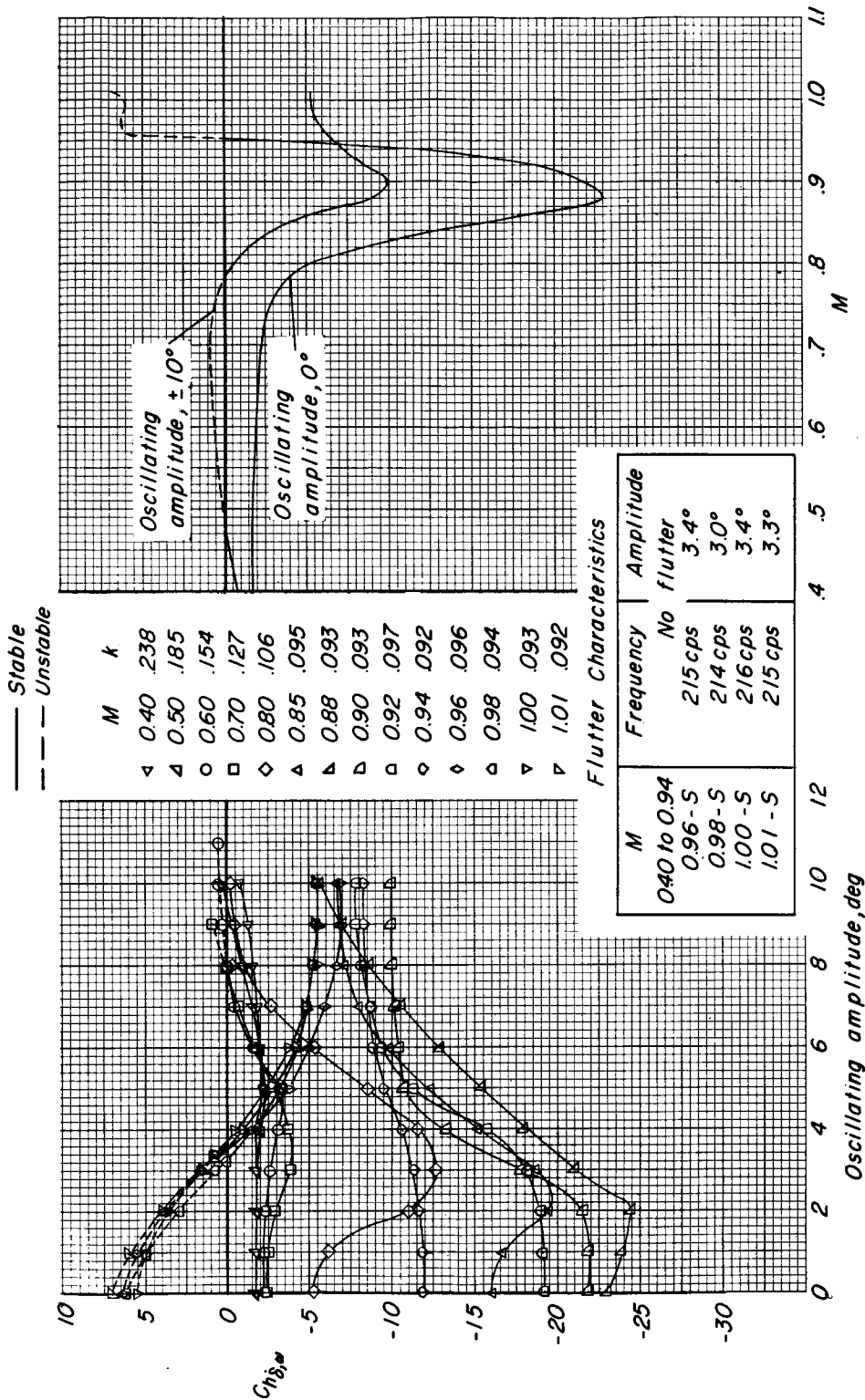
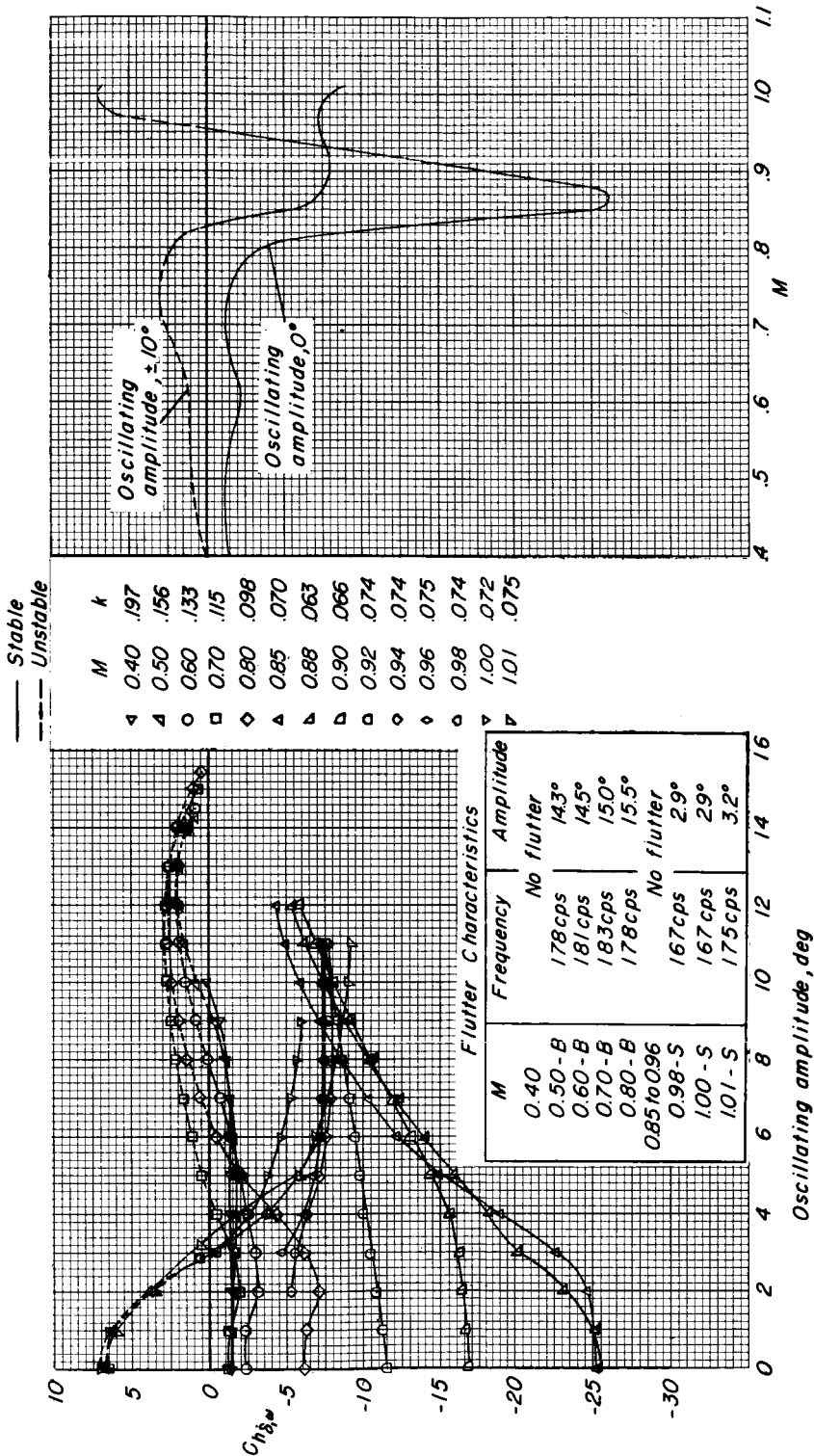
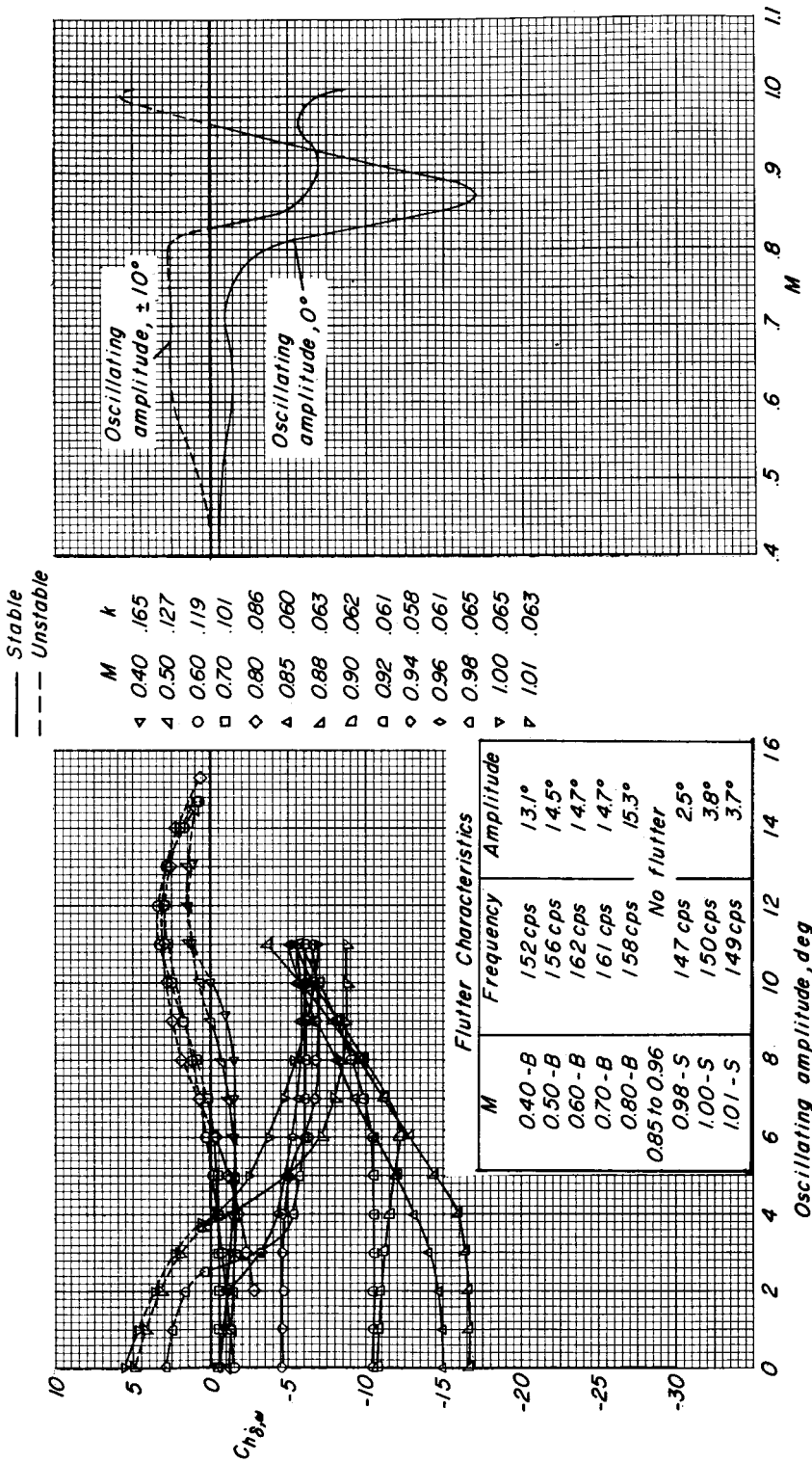


Figure 11.-- Flutter characteristics and variation of aerodynamic damping derivative with oscillation amplitude for various Mach numbers. $c_b/c_a = 1.00$; $\alpha = 0^\circ$.



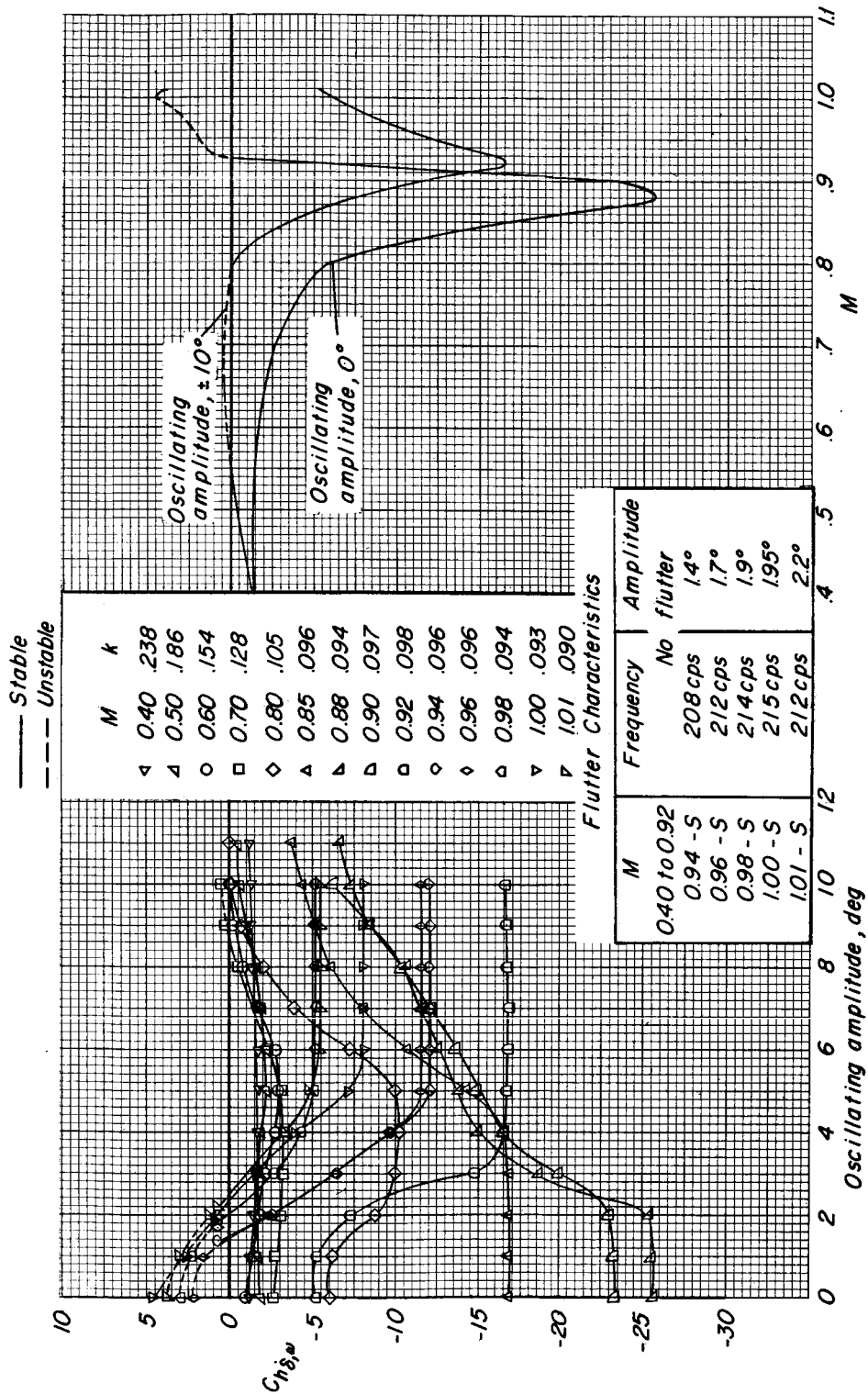
(b) $f_0 = 183$.

Figure 11.- Continued.



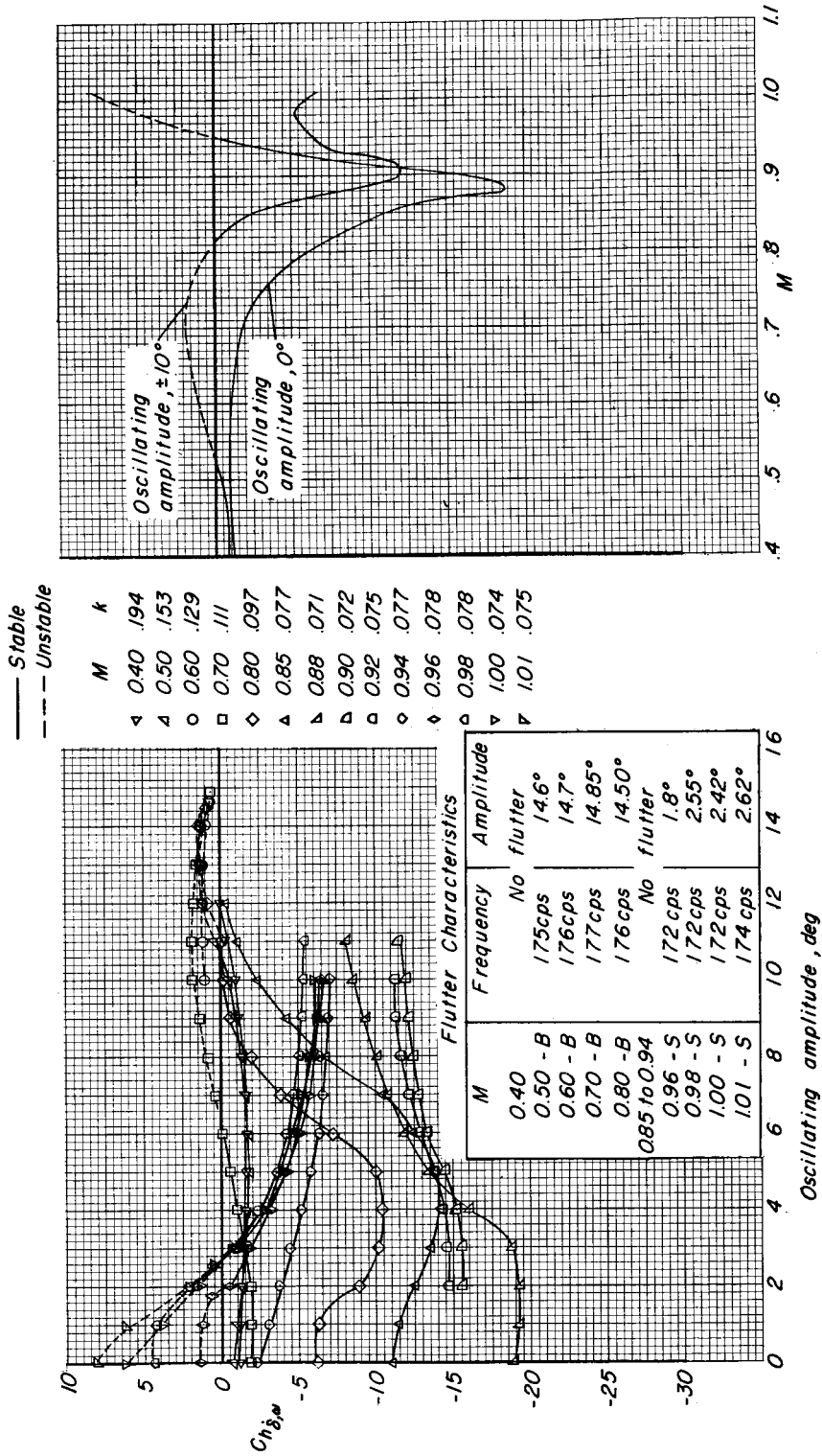
(c) $f_0 = 160$.

Figure 11.- Concluded.



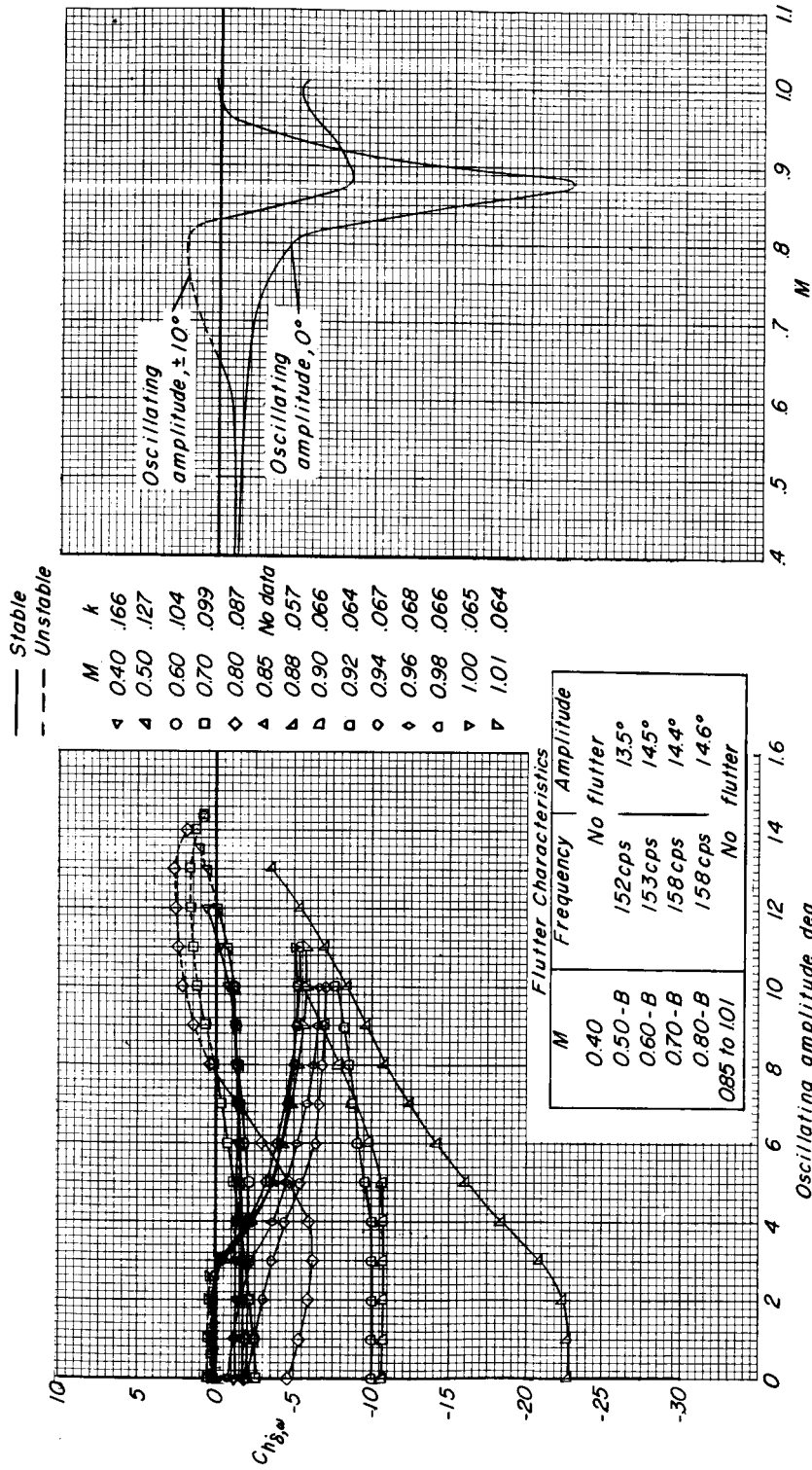
(a) $f_0 = 222$.

Figure 12.- Flutter characteristics and variation of aerodynamic damping derivative with oscillating amplitude for various Mach numbers. $c_b/c_a = 1.00$; $\alpha = 6^\circ$.



(b) $f_0 = 183$.

Figure 12.- Continued.



(c) $f_0 = 160$.

Figure 12.- Concluded.

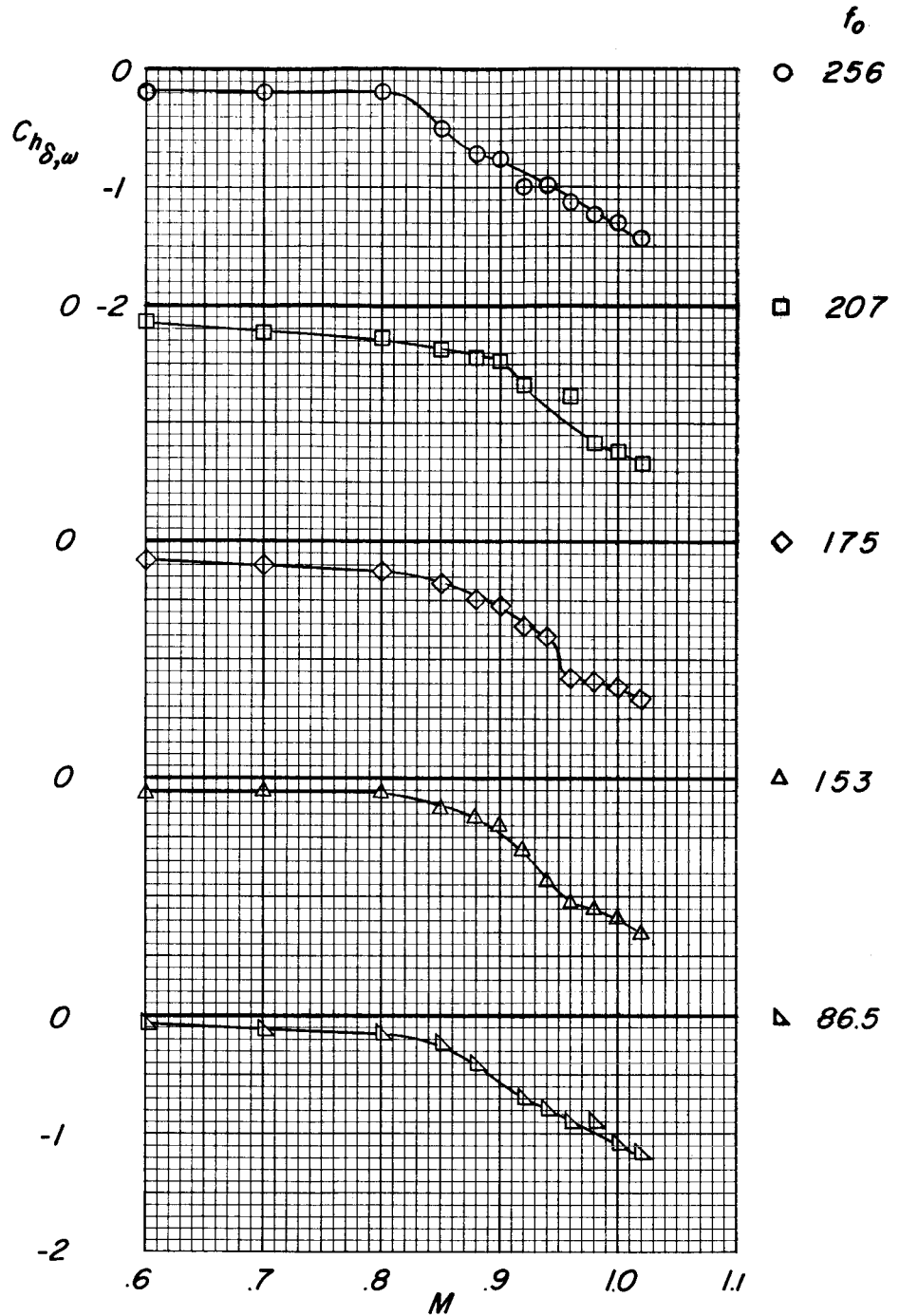


Figure 13.- Variation of aerodynamic spring derivative with Mach number for various control wind-off natural frequencies. $c_b/c_a = 0.35$; $\alpha = 0^\circ$.

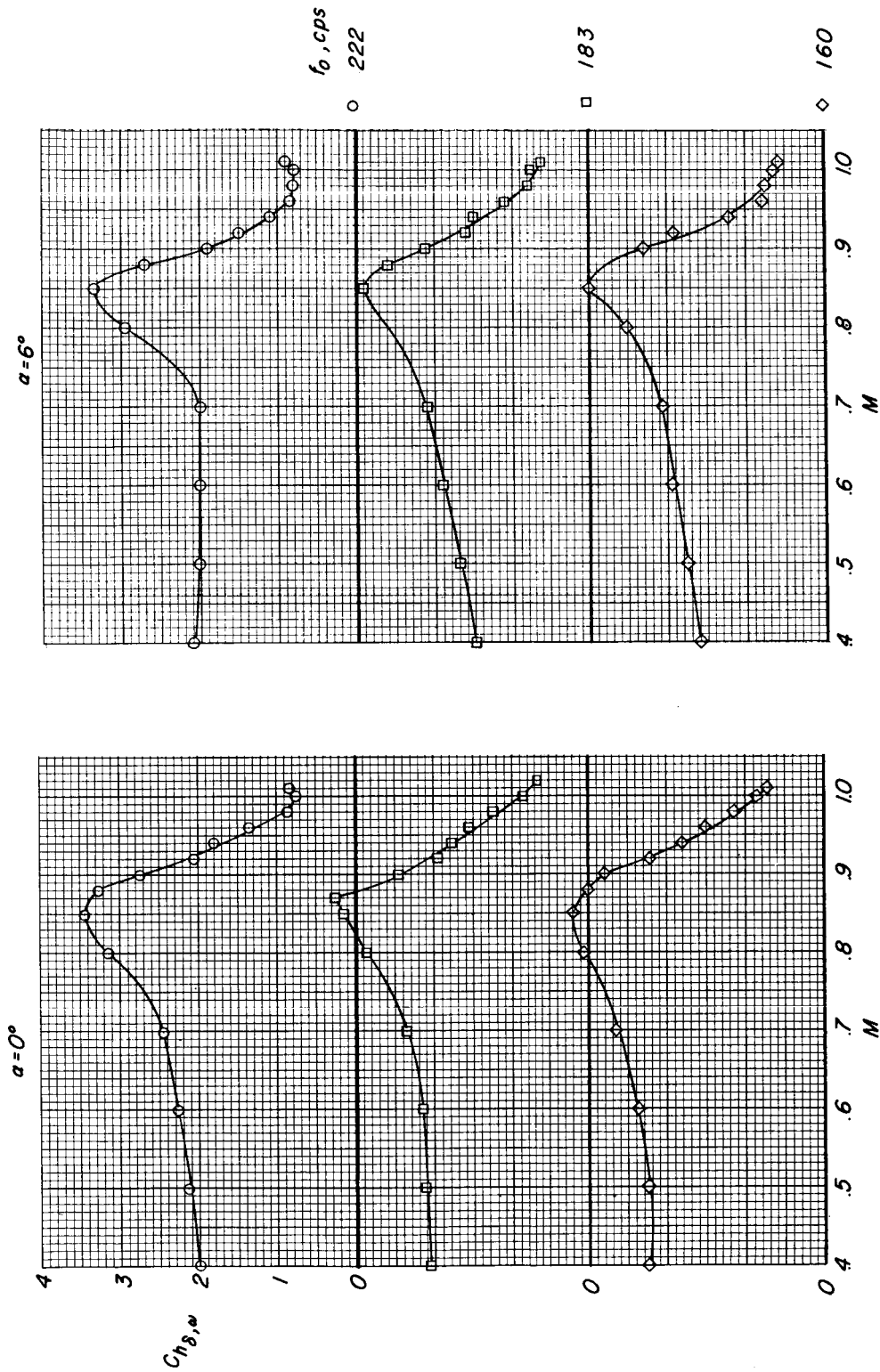
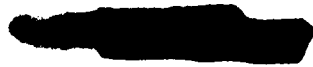


Figure 14.- Variation of aerodynamic spring derivative with Mach number for various control wind-off natural frequencies. $c_b/c_a = 1.00$.



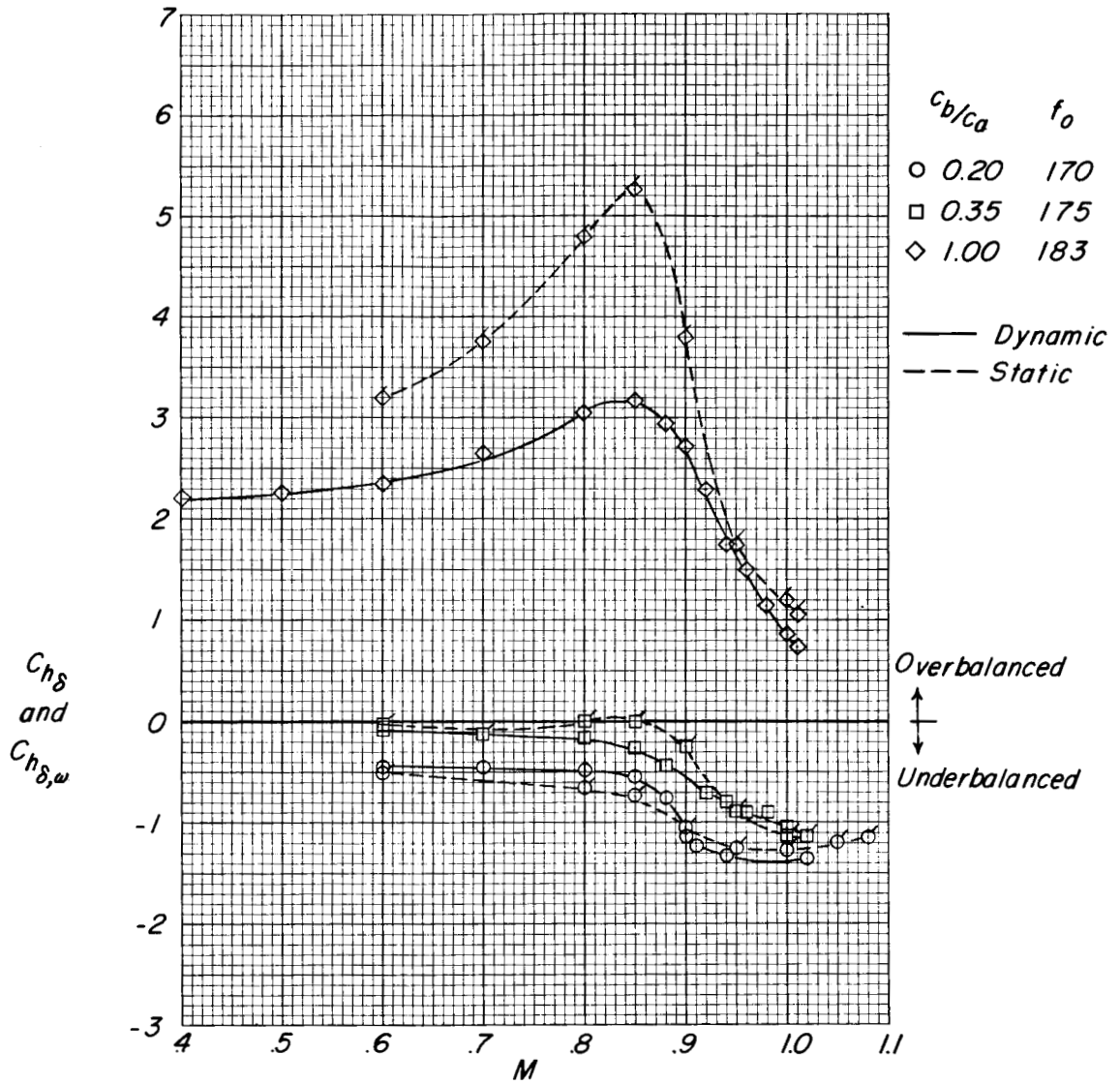
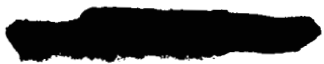


Figure 15.- Comparison of static and dynamic aerodynamic spring derivatives.



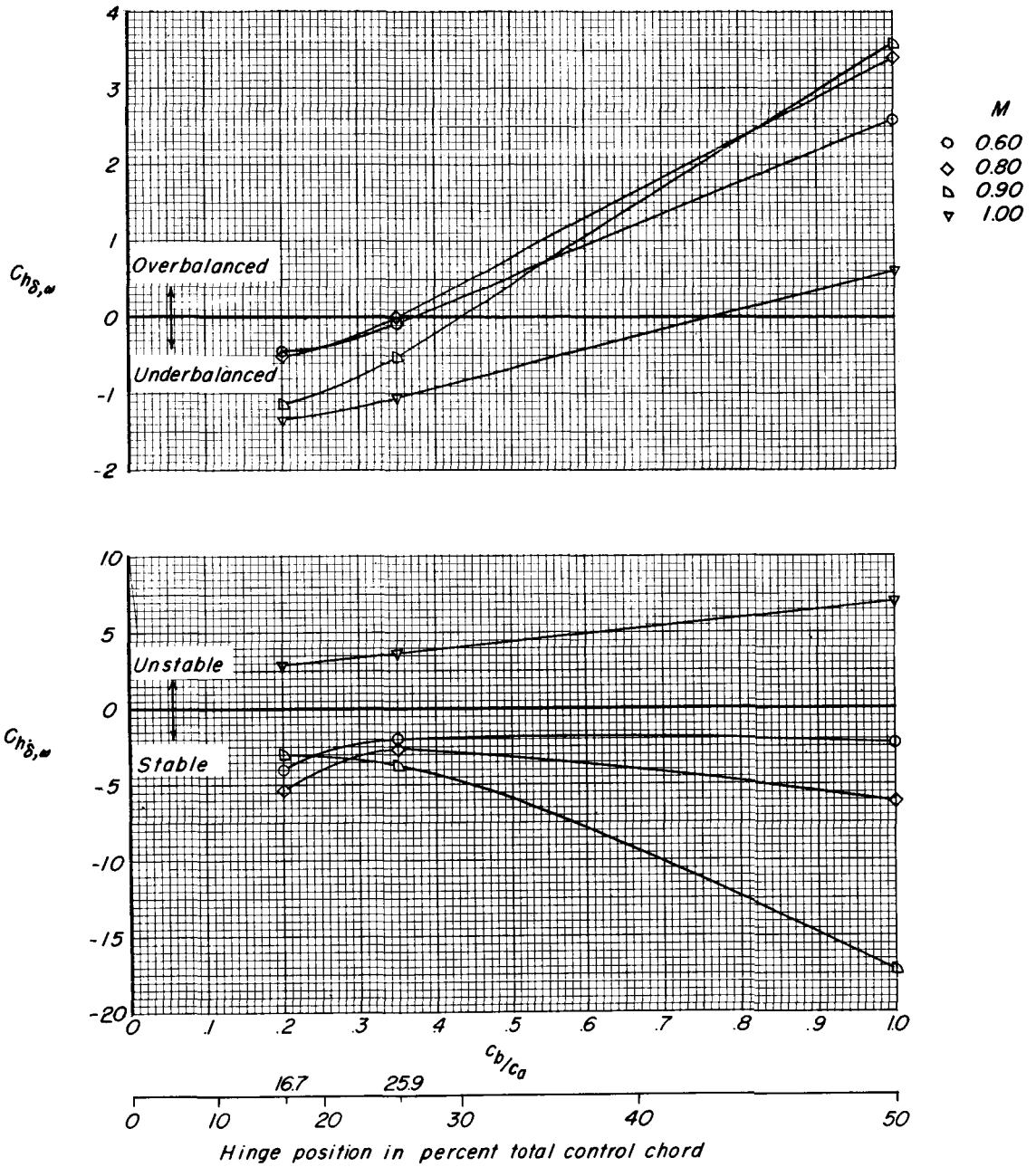
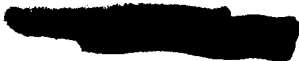


Figure 16.- Effect of control hinge position on the dynamic hinge moment derivatives for representative Mach numbers. $\alpha = 0^\circ$; oscillation amplitude = 1° ; $f_0 \approx 175$.



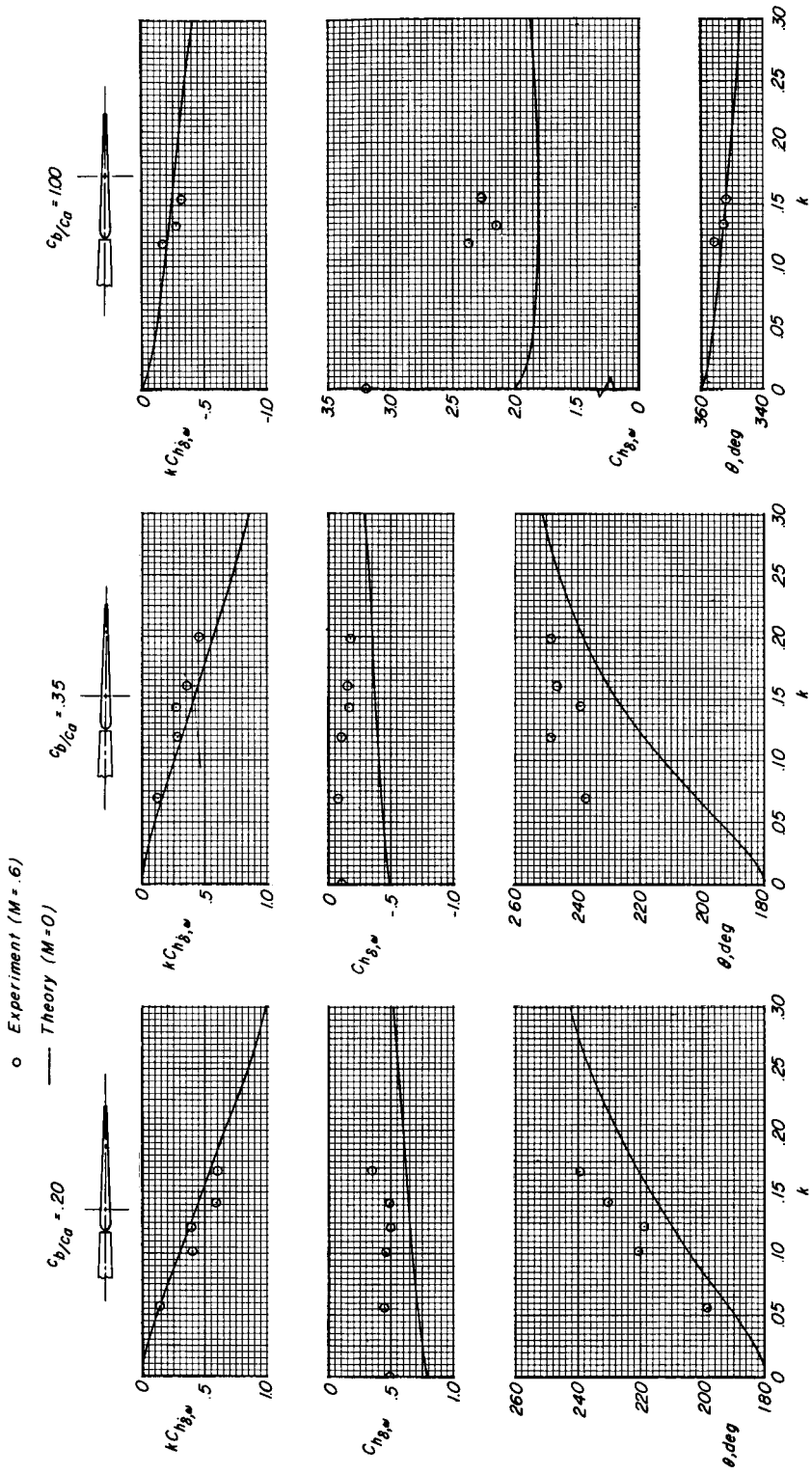
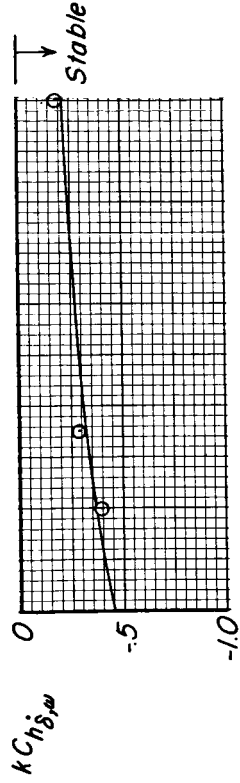


Figure 17.- The effect of control reduced frequency on dynamic hinge-moment parameters and phase angle as determined by experiment and theory for three test hinge-line positions. Oscillating amplitude $\approx 0^\circ$; $\alpha = 0^\circ$.



Dynamic, $k \approx .12$



— Two dimensional theory ($M=0$)
 ○ Experiment ($M=.6$)

Static

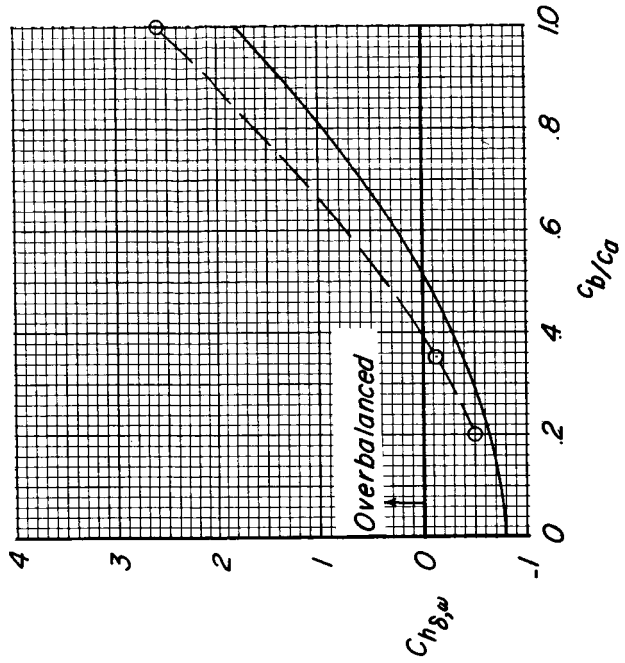
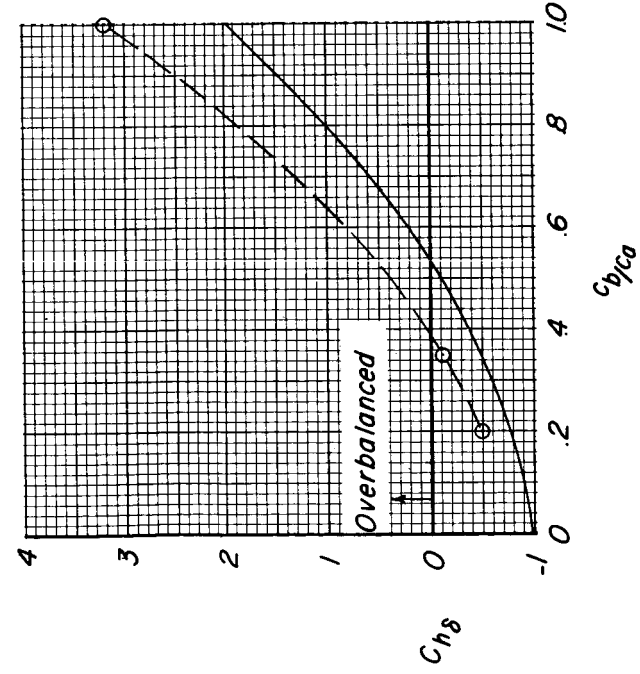
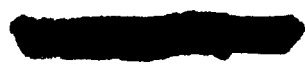


Figure 18.- The effect of hinge-line position on static and dynamic hinge-moment parameters as determined by experiment and theory. $\delta_1 \approx 0^\circ$.



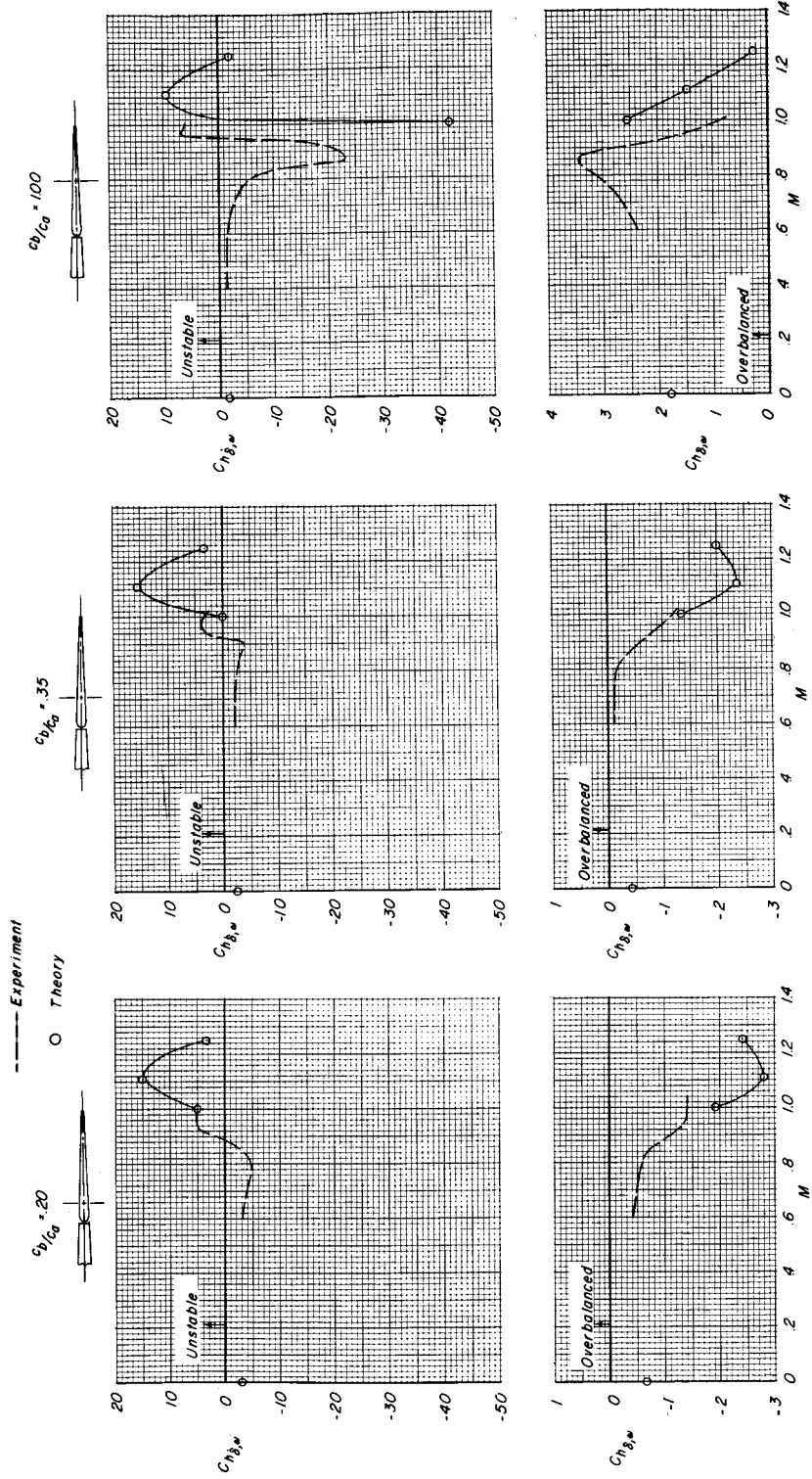


Figure 19.- The variation of experimental hinge-moment derivatives with Mach number compared with results computed by two-dimensional theory for three hinge-line positions. $k \approx 0.10$; $\delta_1 \approx 0^\circ$.

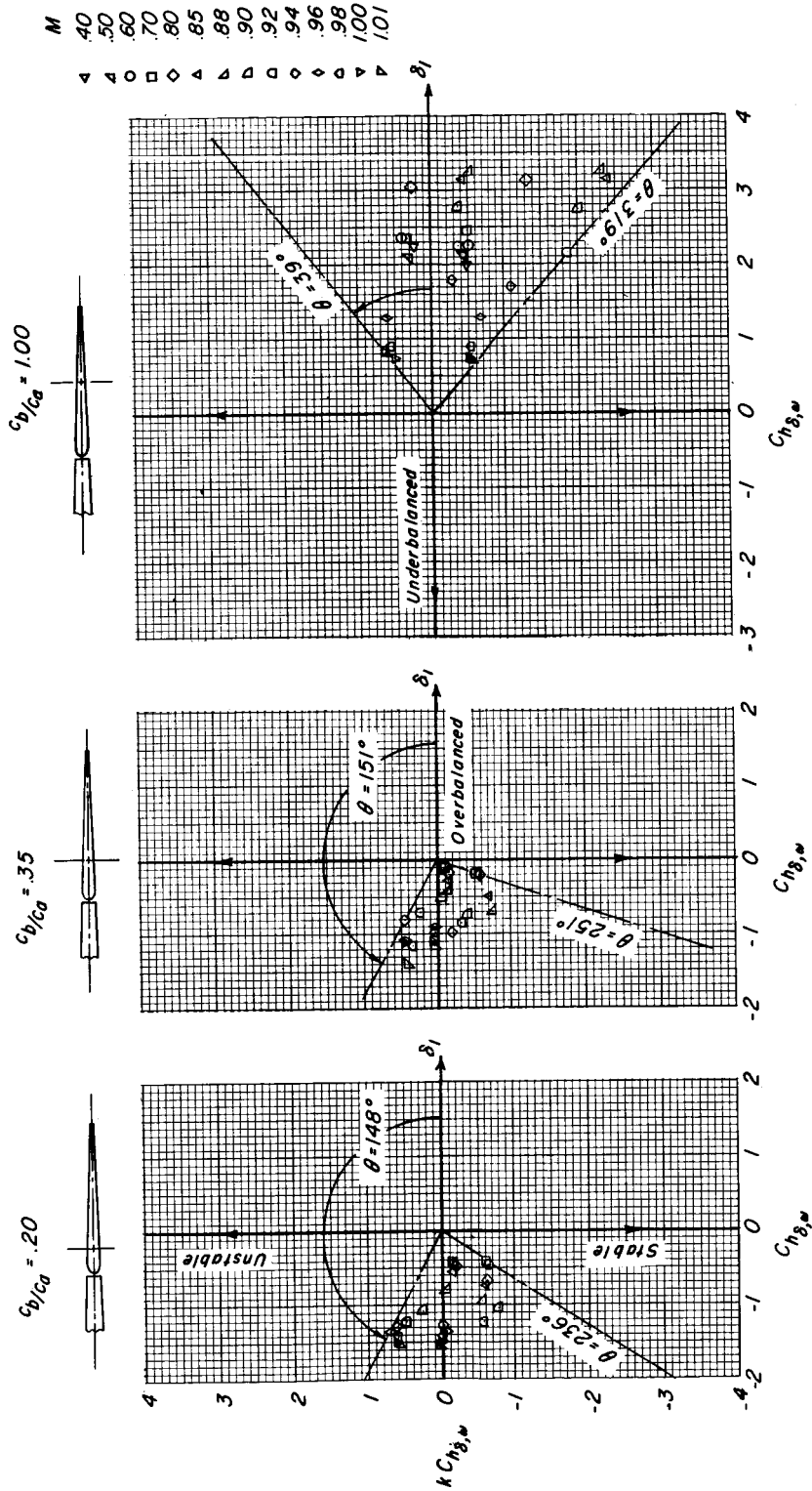


Figure 20.- Vector diagram of the dynamic hinge-moment results for three test hinge-line positions throughout the Mach number and reduced frequency range tested. $\alpha = 0^\circ$.

DECLASSIFIED

CONFIDENTIAL

CONFIDENTIAL

CONFIDENTIAL